THERMODYNAMIC ANALYSIS OF A SINGLE-EFFECT WATER/LiBr VAPOUR ABSORPTION REFRIGERATION SYSTEM

A dissertation submitted

in partial fulfillment of the requirements for the award of the degree of

Master of Engineering

in

Thermal Engineering

By

SANDEEP KUMAR

Roll No: 2206

Under the Guidance of

Dr. R. S. Mishra
Asstt. Professor

Dr. S. S. Kachhwaha
Asstt. Professor

Department of Mechanical Engineering,
Delhi College of Engineering, University of Delhi

Session 2006-07

Candidate's Declaration

I hereby declare that the dissertation entitled on **"THERMODYNAMIC ALALYSIS OF A SINGLE-EFFECT WATER/LiBr VAPOUR ABSORPTION REFRIGERATION SYSTEM"** for the partial fulfillment of the award of the degree of 'Master of Engineering' with the specialization in "**Thermal Engineering"** is the authentic record of my own work carried out under supervision of **Dr. R. S. Mishra** and **Dr. S. S. Kachhwaha,** Department of Mechanical Engineering, Delhi College of Engineering, University of Delhi. I have not submitted the matter in this dissertation for the award of any degree or any other purpose whatever.

Sandeep Kumar
(College Roll No. 09/THR/2005)
University Roll No.2206

Certificate

This is to certify that the above statement by Sandeep Kumar is true to the best of our knowledge and belief.

(Dr R. S. Mishra)
Assistant Professor
Department of Mechanical Engg
Delhi College of Engineering

(Dr S. S. Kachhawaha)
Assistant Professor
Department of Mechanical Engg
Delhi College of Engineering

Acknowledgement

It is a great pleasure to have the opportunity to extent my heartiest felt gratitude to everybody who helped me throughout the course of this dissertation. It is distinct pleasure to express my deep sense of gratitude and indebtedness to my teachers **Dr. R.S. Mishra, and Dr. S.S. Kachawaha,** Department of Mechanical Engineering, Delhi College of Engineering, for his invaluable guidance, encouragement and patient review. His continuous inspiration only has made me complete this project.

I would also like to take this opportunity to present my sincere regards to my teachers for their kind support and encouragement.

I am thankful to my friends and classmates for their unconditional support and motivation for this project.

SANDEEP KUMAR

University Roll No.:2206

CONTENTS

Abstract

Compressor intake air cooling in Gas turbine power plants is considered to be very important and feasible requirement now-a-days. The methods for the compressor intake air cooling are evaporative cooling, vapour compression system, vapour absorption refrigeration system, hybrid system.

In the present work, the focus is upon the thermodynamic analysis of Water/LiBr Vapour Absorption Refrigeration System. The analysis includes Energy and Second Law Analysis of the system. Three different subroutines formulation is given for the prediction of various temperature combinations of the components of the system. The analysis is drawn for a volumetric air flow rate of 86 cu.m/s required for a 30 MW Gas Turbine Power Plant. The Second Law Analysis show that in the total system, the maximum exergy destruction occurs in the evaporator assembly including evaporator, absorber and condenser. The exergy destruction in the total system increases with increase in condenser and absorber temperatures. On the other hand, this rate increases with reduction of evaporator and generator temperatures. The Coefficient of Structural Bonds (CSB) for condenser is 1.04 while for evaporator, absorber and generator CSB is 0.76, 0.69 and 0.31 respectively.

Nomenclature

Notations

C_{pa} Specific heat of air in kJ/kgK

C_{ps} Specific heat of water in kJ/kg K

ė Standard exergy in kW/kmol

f Rich refrigerant concentration solution circulation ratio

h Specific enthalpy in kJ/kg

m Mass flow-rate in kg/s

M Molecular mass of water in kg

P Pressure in kPa

Q_{ex} Heat exchanged in the air heat exchanger in kW

s Specific entropy in kJ/kg K

T Temperature in K

T_{ce} Evaporator temperature in K

T_{hc} Condenser temperature in K

v Specific volume in cu.m/kg

x Concentration of LiBr in Water/LiBr solution in kg-wt.%

Y_D Exergy destruction ratio

Y_L Exergy loss ratio

Greek symbols

η_{ex} Exergetic efficiency

ρ Density of Water/LiBr solution in kg/cu.m

ε Effectiveness of solution heat exchanger

ω Specific humidity of air in kg/kg of dry air

Abbreviations

COP Coefficient of performance

CSB Coefficient of Structural Bonds

E Total exergy in kW

EV Expansion valve

E_D Exergy destruction in kW

Q Heat exchange in kW

T Temperature in K

TV Throttle valve

V Volumetric air flow-rate in cu.m/s

W Work in kW

Superscript

Ph Physical

Ch Chemical

Subscript

a Absorber

atm Atmospheric

D Destruction

e Evaporator

ea Evaporator assembly

ex Exergetic

c Condenser

db	Dry bulb
g	Generator
F	Fuel
fg	Latent
hx	Solution heat exchanger
H2O	Water
in	Inlet
L	Loss
out	Outlet
P	Product
Wb	Wet bulb
0	Reference point (298.15 K)
1-18	States in Vapour Absorption Cycle (see Figure 3.1)

List of Figures

Chapter 1

Chapter 3

Chapter 4

List of Tables

Chapter 3

Chapter 4

Chapter 1
Introduction

1.1 Importance of Cooling

The adverse effect of high ambient air temperatures on the power output of a gas turbine is two fold: as the temperature of the air increases, the air density decreases and consequently the air mass flow. The reduced mass flow directly causes decrease in the power output of the gas turbine. On the other hand the higher intake air temperature results in an increase in specific compressor work. Thus the use of high temperature ambient air results in a net decrease in the gas turbine output.

As shown in the Figure 1.1, turbine power output is a linear inverse function of temperature. The power correction factor is a factor which when multiplied with the power output of gas turbine cycle operating at ambient inlet air conditions will give the corresponding power output at chilled air temperature.

The most common approach utilized in power generation to increase mass flow is to increase the air density by lowering the inlet air temperature. Depending on the type of the gas turbine, the electric output will decrease by-a percentage between 6 and more than 10 % for every 10° C increase of intake air temperature. At the same time, the specific heat consumption increases by a percentage between 1.5 % and more than 4.5 %. It can be concluded that at temperature of 40-45°C, common in India and various other countries where a large number of gas turbines are used for electricity generation, there is a power loss of more than 20%, combined with a significant increase in specific fuel consumption, compared to ISO standard condition (15°C). Thus in summer over a long period of time (April-June), gas turbines demonstrate a lower power output and efficiency than the equipment could actually perform. If it was possible to obtain a constant low inlet air temperature, a constant high power output could be generated from a gas turbine.

Unlike steam turbine cycles which require a very small compressor to turbine work ratio, gas turbine cycles may require back work ratios upto 40 or even 50 % depending essentially upon the compressor inlet air temperature and the extent of compressor intercooling. For a given compression ratio and volumetric flow rate the compressor power is constant while the turbine power decreases with increasing the inlet temperature, therefore, maximizing of net gas turbine power cycle requires the largest feasible value of the turbine to compressor inlet temperature ratio. While the quest for higher gas turbine inlet temperatures and compressor intercooling has been the panacea for higher net power outputs, not as much effort has been devoted to decrease the compressor inlet air temperature except for those modest reductions allowed by adiabatic air cooling of dry and warm air in arid climates. Various techniques of compressor intake air cooling are summarized in the subsequent section.

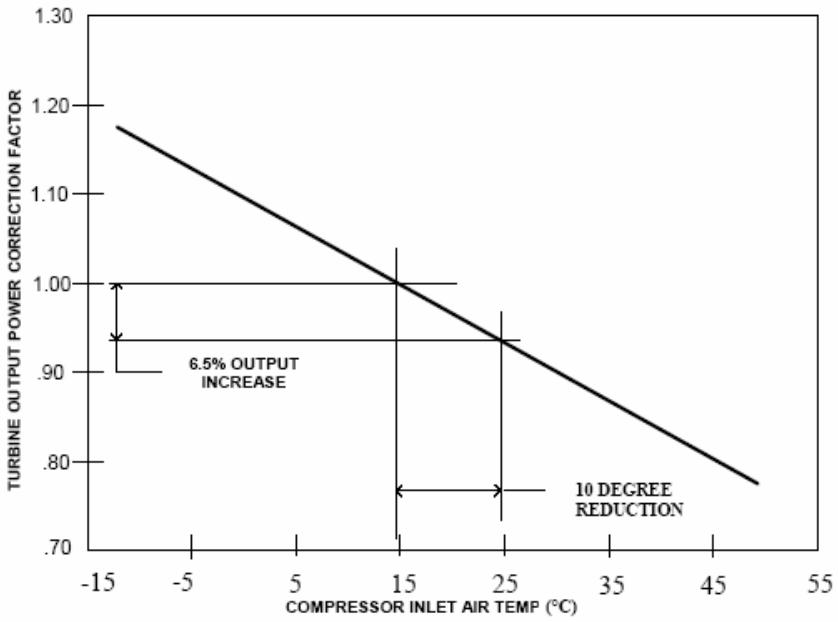

Figure 1.1 System performance curve

1.2 Types of Inlet Air Cooling Methods

There are a number of various popular techniques available to increase the cooling phenomenon of the inlet air to the compressor of a gas turbine. These are described below:

1.2.1 Evaporative Cooling System

Evaporative cooling is based on the evaporation of water injected in the intake air of the gas turbine. As water evaporates, the latent heat of evaporation is absorbed from the water body and the surrounding air. As a result, both the water and the air are cooled during the process. In the limiting case, the air leaves the cooler at a saturated state. The evaporative cooling process is essentially identical to the adiabatic saturation process, since the heat transfer between the air stream and the surroundings is usually negligible. Therefore, the evaporative cooling process follows a line of constant wet-bulb temperature on the psychrometric chart.

Evaporative coolers can be classified into following two types: indirect contact coolers and direct contact coolers. Indirect contact coolers lower the dry bulb temperature without the increased moisture content of inlet supply air, effectively reducing the wet bulb temperature of air and the overall energy content. Direct contact coolers lower the dry bulb temperature as well as increase the moisture content because water is directly fed into the inlet supply air. Direct contact coolers can be further divided into: media based coolers and spray coolers.

Media based evaporative coolers use a corrugated media that is either cellulose or a fiberglass base material. It is a passive system where the material is placed into the air path and wetted via water distribution headers. The construction of this media allows water to penetrate through it and any non-evaporated water returns to a catch basin, and provides sufficient airflow channels for efficient heat transfer and minimal pressure drop.

As air flows through the wetted media, heat exchange occurs. Heat content in the air stream is given up to the wetted media as the air stream absorbs moisture (evaporated water) thereby lowering the inlet air temperature. As shown in the Figure 1.2, a circulating pump transfers the sump water to the distribution manifold. The water splashes down on to a distribution pad then flows down into the media. Due to enhanced surface area, air gets cooled when it comes in contact with water layer. Drift eliminators are utilized to protect the downstream inlet system components from water damage, caused by carry-over of large water droplets.

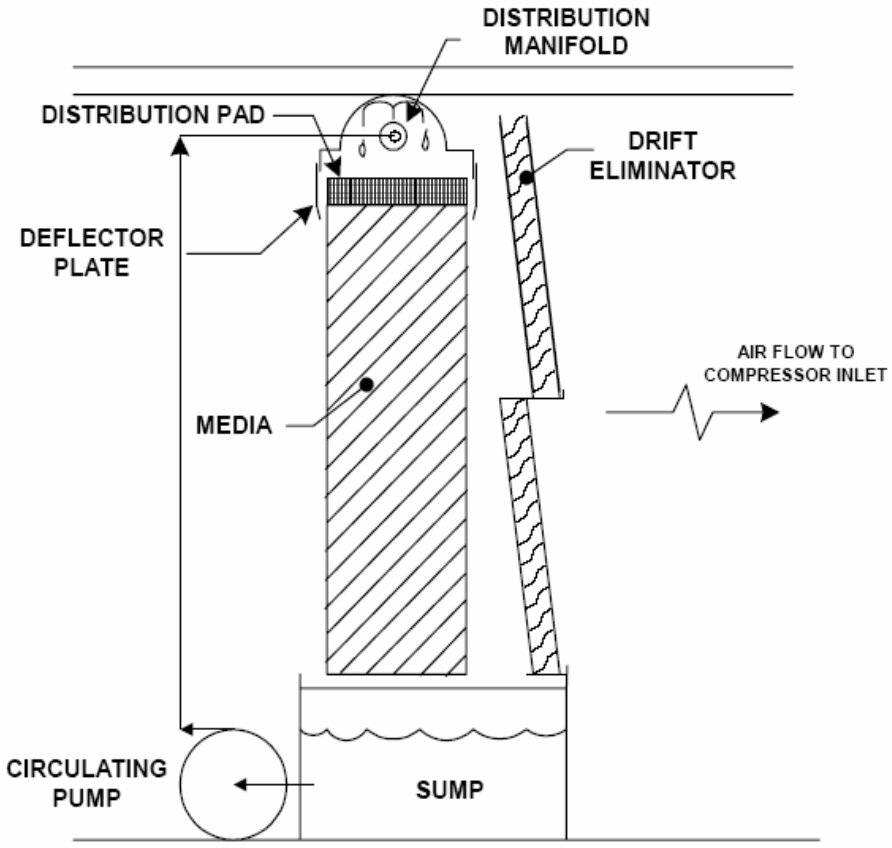

Figure 1.2 Evaporative cooler section (media based)

When designed air velocities across the media are kept below (approximately 3.56 m/s), water distribution rates are maintained generally between 0.001 to 0.002 m^3/s per m^2 of surface area of the distribution pad which is dependant on site conditions, and use

of downstream drift eliminators will form the basis of a system that provides low risk of spray carry-over.

Spray coolers are the closed containers in which cold water is sprayed with the help of injectors. Dry atmospheric air entering into this container adiabatically mixes with spray and becomes saturated. Figure 1.3 shows the simplified schematic of spray cooler. The air enters the system where the water is sprayed into the air stream before it exits from the system. These coolers are based upon the evaporation of water injected in the intake air of the gas turbine. As the water evaporates, the latent heat of evaporation is absorbed from the water body and the surrounding air. As a result both the water and the air are cooled during the process. In the limiting case the air leaves the cooler at a saturated state. The evaporating cooling process is essentially similar to adiabatic saturation process, since the heat transfer between the air stream and the surrounding is usually negligible. Therefore, the evaporative cooling line follows a line of constant wet bulb temperature on the psychrometric chart without gain or loss of heat. The psychrometric process path is shown in Figure 1.4 as process line 1-2 (85% effectiveness) and occurs along the wet bulb/constant enthalpy line. Process line 1-3 shows the adiabatic saturation process (100% effectiveness).

The gain from the use of an evaporative cooler depends upon the relative humidity of the ambient air and it is high for dry ambient conditions, whereas the gain for wet ambient conditions is low. This indicates that this type of intake air-cooling could mainly be of interest in countries where the climate is hot and dry. Furthermore, these coolers are limited by the amount of moisture in the air. Once saturation is reached, evaporative cooling systems are unable to further evaporate water into the air stream. For this reason, in the hot and humid regions, it is not often possible to accomplish more than about 5.5 to 8.5°C of cooling.

1.2.2 Fogging System

High-pressure fogging systems have been used to cool the inlet air to gas turbines and thus increase the power output since the 1980's. Recently this technology has been applied to larger and more efficient industrial gas turbine technology. The compressor blades for modern engines use advanced aerodynamic techniques resulting in a highly efficient compressor. The presence of free water in the air stream can cause erosion and performance impacts, and therefore must be minimized. A typical system is shown in Figure 1.5 and described below:

Demineralized water is injected through a fogging pump skid and a series of distribution manifolds which contain multiple nozzles to distribute the water in the incoming air in small droplets. Many nozzle product offerings claim 90% of the droplets are 20 microns or less, however test techniques vary substantially and comparison of laboratory tests is not straightforward. Hence, performance of the nozzles is critical to the proper operation of the fogging system. The manifolds are located to allow for the longest possible residence time to achieve complete evaporation without lengthening the duct. The incoming air is passed through a filter section (in order to clean it) before the high pressure demineralized water is injected into it through a fogging nozzle array located in the clean plenum. The outgoing air is then passed through the silencer followed by the main compressor, combustor and finally the gas turbine. The injection rate is controlled by the comparison of the ambient wet bulb temperature and compressor inlet air dry bulb temperature through instrumentation located in the weather station. The system runs a series of various sized pumps to increase the flow rate in nominal increments.

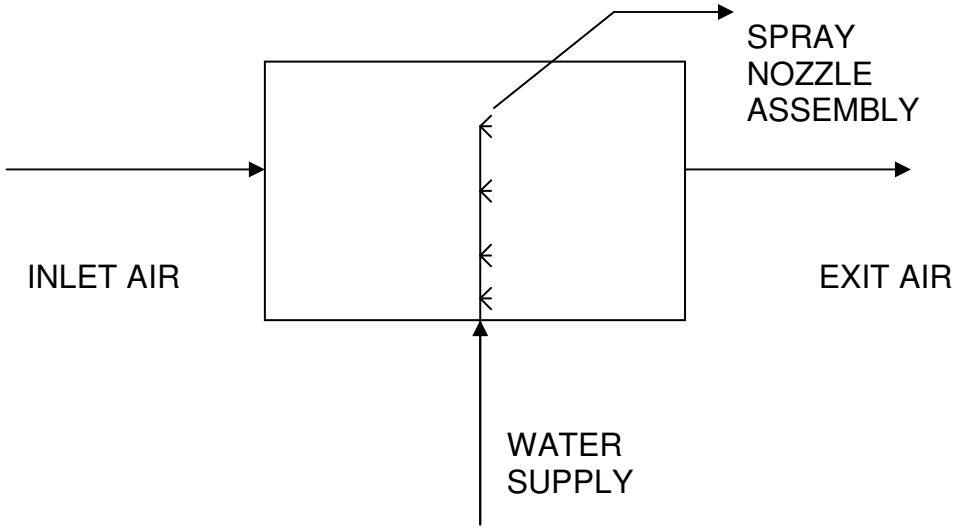

Figure 1.3 Evaporative spray cooler

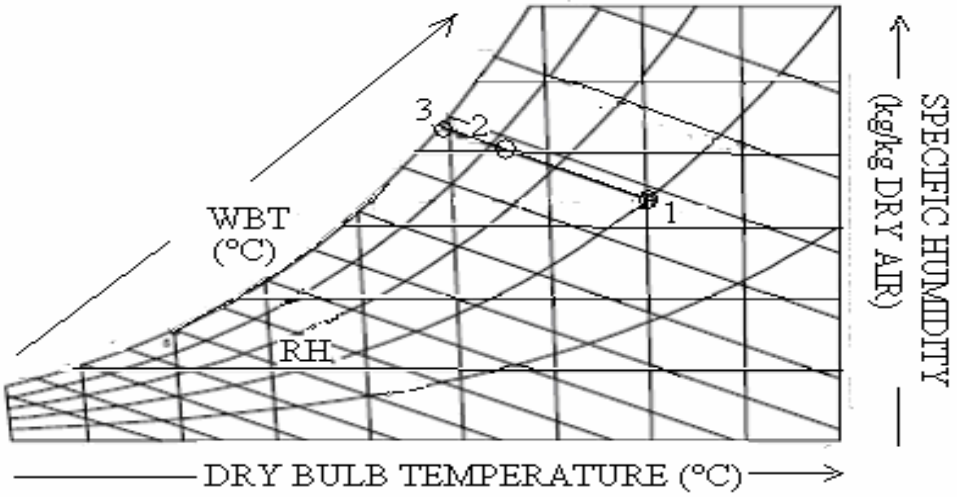

Figure 1.4 Evaporative cooling process on psychrometric chart

As the air stream approaches saturation it takes incrementally more time to evaporate the remaining water particles. It therefore becomes impractical to attain saturation temperature at the inlet without potential overspray.

Calculated flows based on ambient wet bulb temperature and dry bulb temperature are not applied as the primary control variable in the control scheme for these installations since water collected in drains or ingested by the gas turbine are not evaporated, and therefore do not contribute cooling. A secondary default flow limit is calculated from the ambient conditions i.e, wet bulb temperature (T_{wb}) and dry bulb temperature (T_{db}) and set as a failsafe limit for water injection.

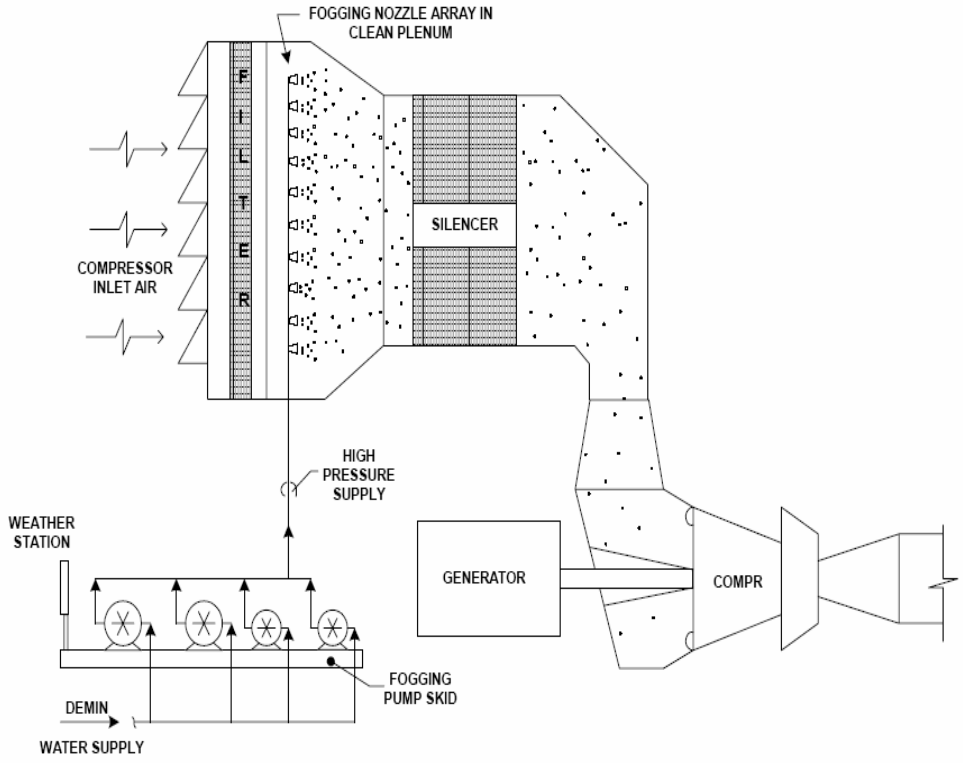

Figure 1.5 Typical fogging system diagram

Observations and test experience have verified that obstructions in the inlet system cause water particle agglomeration, which pool at the inlet. Inlet filter geometry and nozzle arrangement effect the even distribution of the injected fog and contribute to the drainage as the inlet air becomes humid and limited in its capacity to evaporate additional water. While increasing the injection rate would continue to reduce the temperature of the warmer areas, the areas already near saturation would evaporate very little additional water and would contribute significantly to the drainage flow.

The amount of power increase is largely determined by the ambient conditions. Lower available cooling [T_{db}-T_{wb}] tends to degrade the cooler effectiveness. A closer dry bulb approach to saturation is realized in certain high relative humidity applications for media based coolers, but in most instances inlet fogging systems will outperform the media based evaporative cooler. A secondary benefit of staged pump control is its adaptability for load control. Water carry-over (overspray) is of concern and can be minimized through controlled staged pumping to match ambient conditions. Overspray has potential for compressor blade erosion. Fogging pump skids are compact, require minimal service clearances and easily fit into a plant's general arrangement. Fogging systems use demineralized water and therefore require downstream stainless steel inlet duct components. Stainless steel distribution piping is to be considered.

1.2.3 Vapour Compression (V-C) System

Vapour Compression System is shown in Figure 1.6. This system comprises mainly of the following components: evaporator, compressor, condenser and throttle valve. Figure 1.7 shows the temperature (T) versus entropy (s) diagram for the system. The evaporation of the refrigerant inside the evaporator takes place at a constant temperature and pressure (process a-b). Evaporation process is followed by a compression process (process b-c') which in ideal case (b-c) is assumed to be isentropic. The condensation of high pressure and temperature refrigerant vapour leaving compressor takes place inside condenser at a constant pressure (process c'-d). Finally, the high pressure liquid refrigerant is supplied to lower pressure evaporator through throttle

valve (process d-a) for recycling. Figure 1.8 shows the pressure (P) versus specific enthalpy (h) diagram for the system. On the psychrometric chart, the chilled fluid cooling coil process line is indicated in process line 1-2, as shown in Figure 1.9. As inlet air passes over the chilled coil, the water vapor content (humidity ratio) remains constant and the temperature decreases up to the saturation curve. If the inlet air is cooled further, the process line follows the saturation curve and water vapour will be condensed out of the inlet air.

As shown in the Figures 1.6 to 1.8, evaporator absorbs the heat from the inlet air and vaporizes at a lower temperature, thus decreasing the temperature of the air coming out. The vapour after being compressed in compressor is sent to condenser where it loses its latent heat and converts into the liquid phase. The condenser is simultaneously cooled by cooling water flow through it. The liquid refrigerant is throttled through a throttle

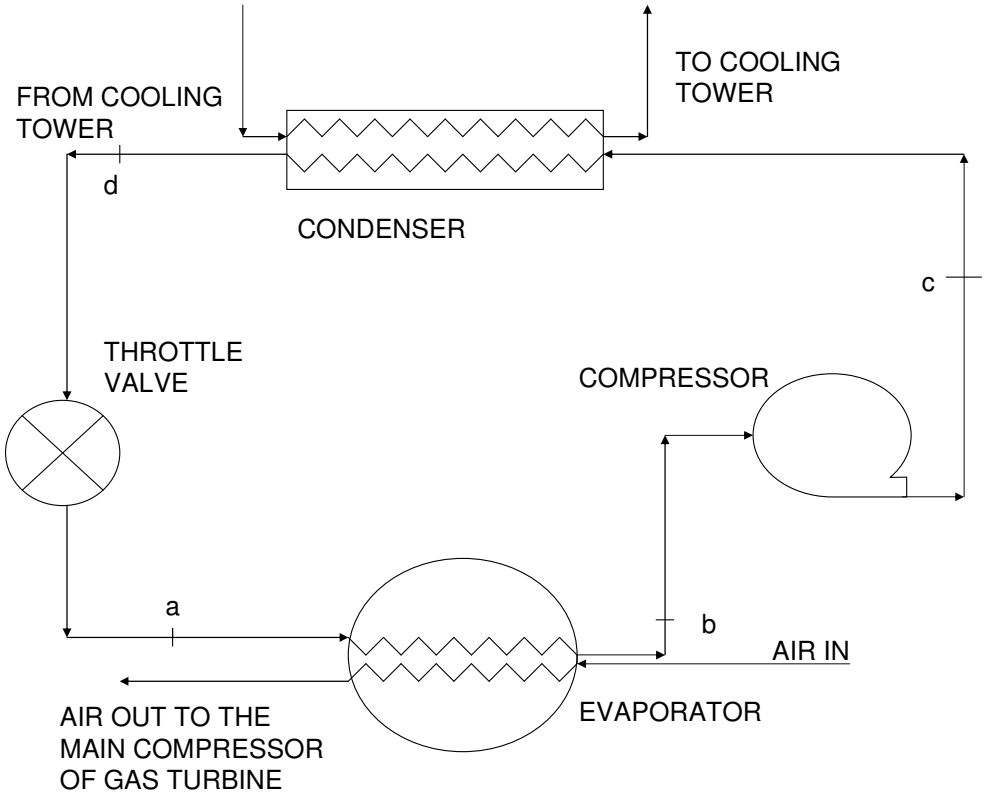

Figure 1.6 Vapour compression system

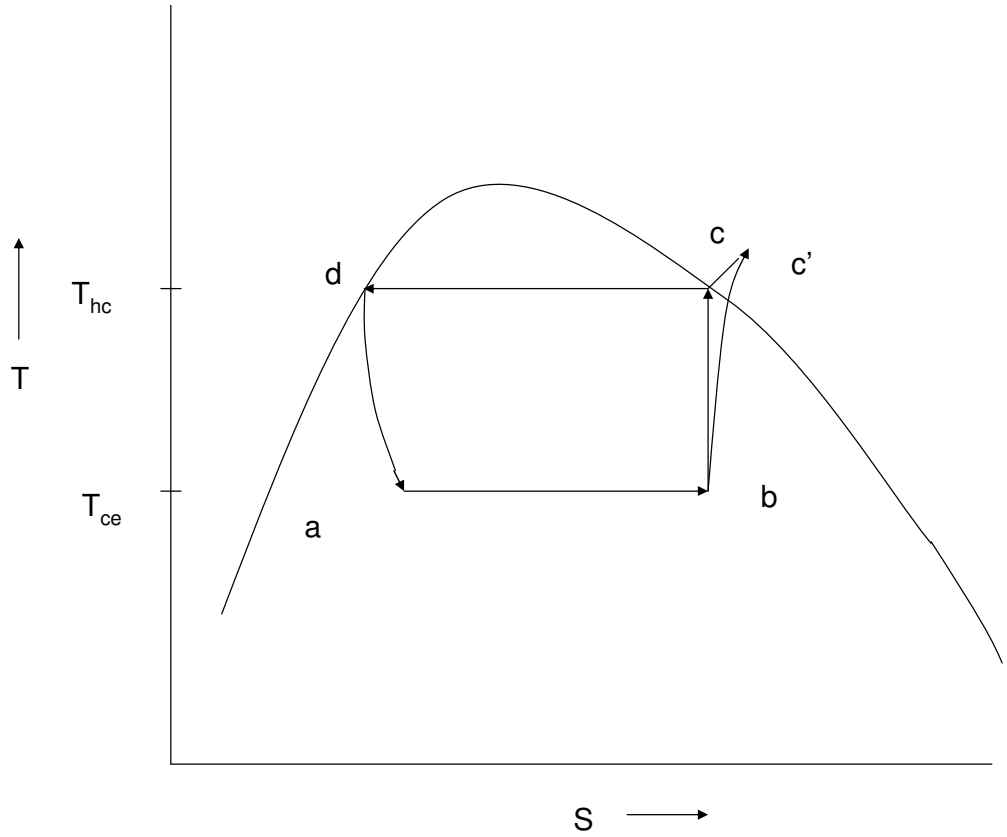

a-b: Isothermal and isobaric evaporation process

b-c: Isentropic wet compression process

b-c': Actual compression process

c'-d: Isobaric condensation process

d-a: Isentropic throttling process

Figure 1.7 Temperature (T) vs. entropy (s) diagram for vapour compression cycle

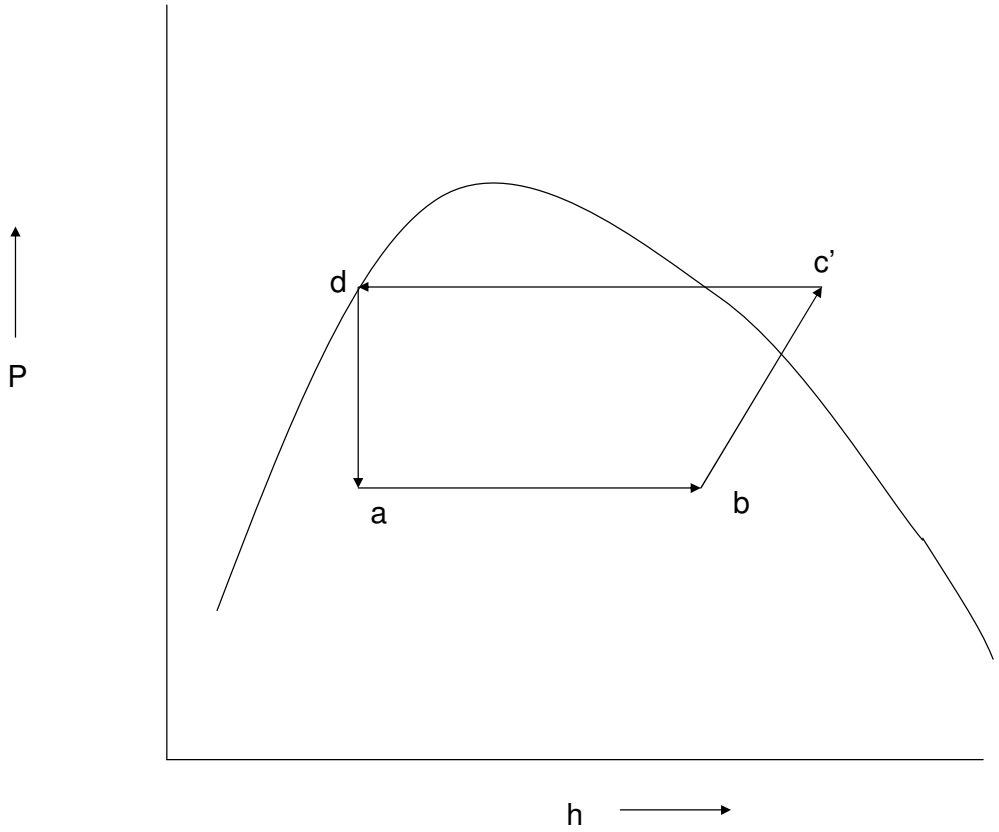

a-b: Isothermal and isobaric evaporation b-c':Actual compression process process

c'-d: Isobaric condensation process d-a: Isentropic throttling process

Figure 1.8 Pressure (P) vs. enthalpy (h) diagram for vapour compression cycle

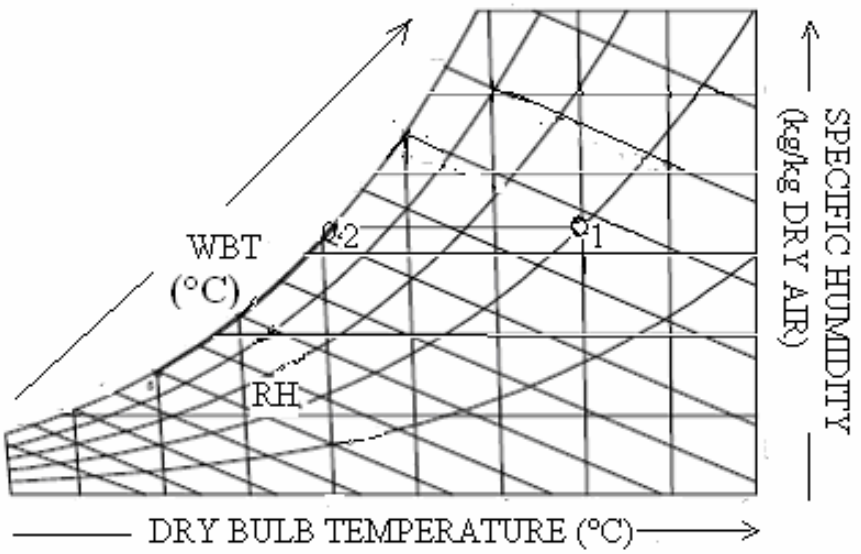

Figure 1.9 Vapour compression process on psychrometric chart

valve so that the refrigerant pressure is reduced to the evaporator pressure and the enthalpy remains constant. The cooled air coming out of the evaporator is supplied to the main compressor of the gas turbine cycle. As a result the power output of the cycle is increased.

1.2.4 Vapour Absorption Refrigeration (VAR) System

In the vapour absorption refrigeration system, the function of the compressor is accomplished in a three-step process by the use of the absorber, pump and generator. Absorber forms a strong or rich solution by the absorption of the refrigerant vapour by its weak or poor solution in a suitable absorbent or adsorbent. Pump serves the purpose of pumping the rich solution raising its pressure to the condenser pressure. Generator or desorber distillates the vapour from the rich solution leaving the poor solution for recycling.

An absorption chiller system, therefore, consists of eight components viz., generator, condenser, evaporator, absorber, pump, heat exchanger, throttle valve and expansion valve as shown in Figure 1.10. The refrigerant is vaporized in the evaporator after taking heat from the ambient air. It is then sent to the absorber where the refrigerant vapours get condensed. During the process, latent heat liberated during condensation of refrigerant vapours is taken by the circulating cooling water in absorber. The solution coming from absorber and rich in refrigerant concentration is pressurized through pump upto generator pressure where it is heated to give off refrigerant vapour, forming weak concentration refrigerant solution. This weak concentration refrigerant solution then returns to absorber and mixes with refrigerant vapours coming from evaporator, forming a strong concentration refrigerant solution which is then re-circulated in the circuit. The refrigerant vapours are condensed in the condenser liberating heat of condensation. The function of heat exchanger is to heat up the strong concentration refrigerant solution entering generator by hot and poor concentration refrigerant solution leaving generator. Throttle valve and expansion valve are used to reduce the pressure of poor concentration refrigerant solution and refrigerant coming out from condenser to absorber and evaporator pressure respectively. The heat is supplied to the generator by high temperature steam or hot water entering the generator through the generator coils. The heat rejected in the condenser is passed to the circulating cooling water which in turn gets heated up and finally transferred out off the system for further use. Both, condenser and evaporator are generally maintained under vacuum. The great advantage of this type of cooler is that the intake air can be cooled to a specific temperature for a wide range of temperatures and therefore the power output of a gas turbine plant can remain constant, independent of ambient air conditions.

Some of the desirable characteristics of a refrigerant-absorbent pair for an absorption system are low viscosity to minimize pump work, low freezing point and good chemical and thermal stability. Irreversible chemical reactions of all kinds, such as decomposition, polymerization, corrosion, etc., are to be avoided.

In addition to the above, two main thermodynamic requirements of the mixture are:

(a) *Solubility requirement:* The refrigerant should have more than Raoult's law solubility in the absorbent so that a strong solution, highly rich in the refrigerant, is formed in the absorber by the absorption of the refrigerant vapour.

(b) *Boiling points requirement*: There should be a large difference in the normal boiling points of the two substances, at least 200°C, so that the absorbent exerts negligible vapour pressure at the generator temperature. Thus, almost absorbent-free refrigerant is boiled off from the generator and the absorbent alone returns to the absorber.

The two commonly used refrigerant-absorbent pairs are: Water/lithium bromide (H_2O/LiBr) absorption refrigeration system and Ammonia/Water (NH_3/H_2O) absorption refrigeration system. H_2O/LiBr absorption chiller system can produce cooling only up to 0°C while the later one can easily produce cooling up to -50°C. In the gas turbine power plants, LiBr-H_2O absorption chiller system is usually favoured because of economy and hazard consideration.

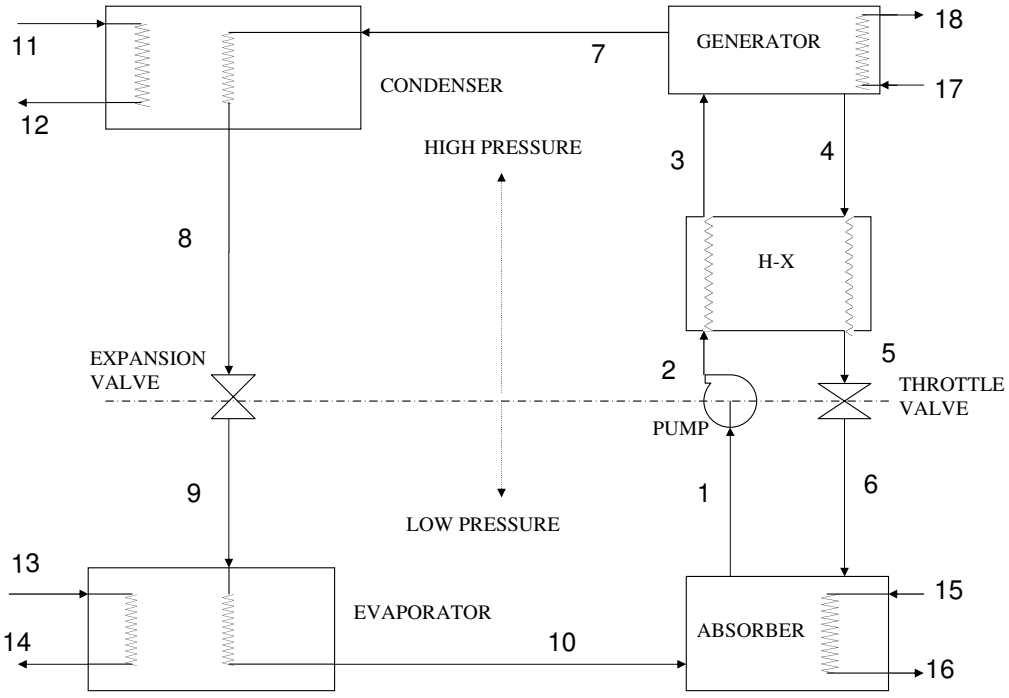

1-Strong water concentration LiBr solution leaving absorber

2-Strong water concentration LiBr solution entering heat exchanger

3-Strong water concentration LiBr solution leaving heat exchanger

4-Weak water concentration LiBr solution leaving generator

5-Weak water concentration LiBr solution leaving heat exchanger

6- Weak water concentration LiBr solution entering absorber

7-High pressure water vapour

8-High pressure water

9-Low pressure water

10-Low pressure water vapour

11- Cooling water in

12- Cooling water out

13-Air in

14-Air out

15-Cooling water in

16- Cooling water out

17- Hot water in

18- Hot water out

Figure 1.10 Vapour absorption refrigeration system

In the Water/lithium bromide system, water is the refrigerant and lithium bromide the absorbent. Hence, the mixture is used only in air-conditioning applications. The mixture is non-ideal and is satisfactory from the point of view of solubility requirement . Since lithium bromide is a salt, it exerts no vapour pressure. So, the vapour leaving the generator is a pure refrigerant. The mixture also satisfies the boiling point requirements. However, it is corrosive and the plant works under high vacuum.

In the Ammonia/Water system, ammonia is the refrigerant and water the absorbent. Ammonia forms a highly non-ideal solution in water. Hence, it is satisfactory from the point of view of the solubility requirement. But the difference in their boiling points is only 138°C. Hence, the vapour leaving the generator contains some amount of water which results in many problems. Thus, the Ammonia/Water system is not suitable from the point of view of the boiling point requirement. The system is similar to the system shown in Figure 1.10 with only difference that analyzer and rectifying column are installed over generator in order to remove any absorbent vapour coming to generator.

Water/LiBr vapour absorption refrigeration system can be further classified as: single stage Water/LiBr absorption chiller and double-stage-double-effect Water/LiBr absorption chiller. As shown in Figure 1.11, the single stage chiller design utilizes a single shell hermetically sealed construction. These chillers operate on low pressure saturated steam. The saturation pressure in the generator is approximately within 5.6-101.325 kPa (80-120°C). Condenser and evaporator saturation pressures are approximately 5.6-7.37 kPa (36-40°C) and 0.65-1.2 kPa (1-10°C) respectively. The temperature in generator is never allowed to exceed 120°C to avoid corrosion problem. The system operates at vacuum and may be susceptible to air leakage, which could cause some damage. However if proper operating and maintenance procedures are followed, there should be no problem during normal operation.

The main objective of a higher effect cycle is to increase system performance when high temperature heat source is available. By the term “double-effect”, the cycle

has to be configured in a way that heat rejected from a high-temperature stage is used as heat input in a low-temperature stage for generation of additional cooling effect in the low-temperature stage. As shown in Figure 1.12, high temperature heat from an external source (steam) supplies to the first-effect generator. The vapour refrigerant generated is condensed at high pressure in the second-effect generator. The heat rejected is used to produce additional refrigerant vapour from the solution coming from the first-effect generator (through heat exchanger 2 and throttle valve). The remaining solution, weak in water concentration, is then circulated to absorber through heat exchanger 1. The system configuration is considered as a series-flow-double-effect absorption system.

The double-stage-double-effect LiBr-water absorption chiller system operates with a higher saturated steam pressure of approximately 550 kPa (157°C) allowing the unit to consume less steam than a single stage system. This system is considered as a combination of two single stage absorption systems. The coefficient of performance of this system is 0.96 when the corresponding single stage system has the value of 0.6. On the other hand the cost of the system is approximately 30 percent more than a single stage system.

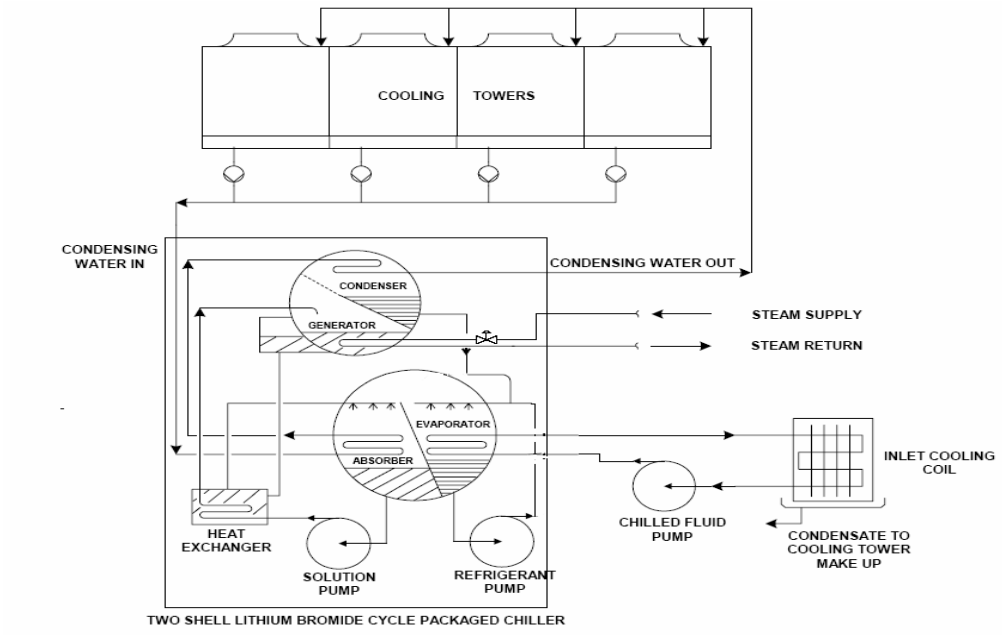

Figure 1.11 Typical absorption chilling schematic

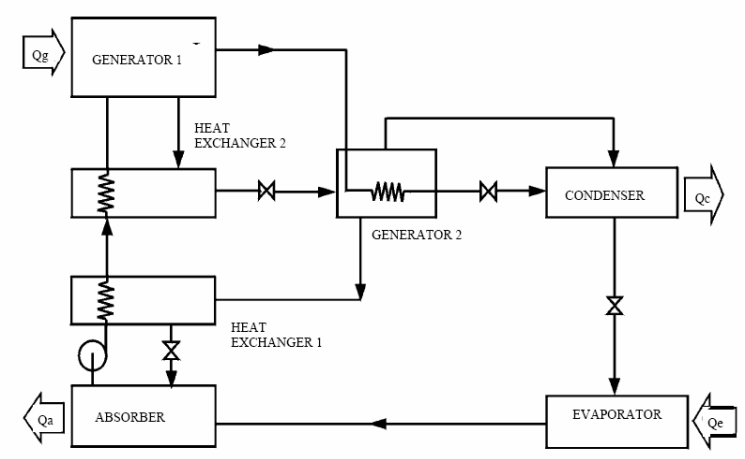

Figure 1.12 Double-stage-double-effect Water/LiBr absorption chiller system

1.2.5 Hybrid system utilizing Absorption Chiller and Vapour Compression System

As shown in Figure 1.13, this hybrid system is a combination of the Water/LiBr VAR and the mechanical centrifugal chiller (vapour compression) system. The Water/LiBr system chills the return water (approximately by 10°C) and the mechanical chiller further reduces the temperature by approximately 6°C. This is a series type system: two 50 percent capacity trains of absorption and vapour compression chiller systems. This system initially takes advantage of the steam available at the facility and enables the mechanical chillers to consume less power during the production of colder chilled water. The system is sized for one-half of the cooling by absorption and the other by centrifugal chilling, which consumes approximately one-half of the total required power than the mechanical chiller system. The chilled water supply increases the temperature differential of the cooling coil inlet and outlet. The larger differential temperature reduces the overall chilled water flow rate, reducing pumping costs as well

as piping requirements. The lower chilled water temperature can be used in the gas turbine cycle inlet air coils to cool the air from 35°C to 12°C or to 6°C. Application of the hybrid system results in lower chilled water temperatures in the chilled water system associated with less piping and pumping costs. Also, the cooling coils are more effective, decreasing the overall size requirements.

The chilled water distribution system circulates chilled water (approximately at 7°C) from the chilled water plant into gas turbine inlet filter house and return with increased temperature (approximately 17°C) water. The inlet cooling coil system distributes the chilled water through an indirect or a direct contact heat exchanger that should be installed across the inlet airflow cross section.

The inlet cooling system chills the inlet ambient air temperature from 35°C and 30 percent relative humidity to 12°C and 95 percent relative humidity. This chilling effect removes both sensible and latent heat, the later producing condensed water at an approximate rate of 0.0009 cu.m/s. The increased humidity in this system increases the corrosion rate of steel components of gas turbine inlet air system

1.2.6. Hybrid System utilizing Evaporative Cooling and Absorption Chiller System

As shown in Figure 1.14, this hybrid system consists of two parts:

(1) A direct contact air-cooler.

(2) A specially designed LiBr absorption chiller capable of producing chilled water at temperatures as low as 2°C.

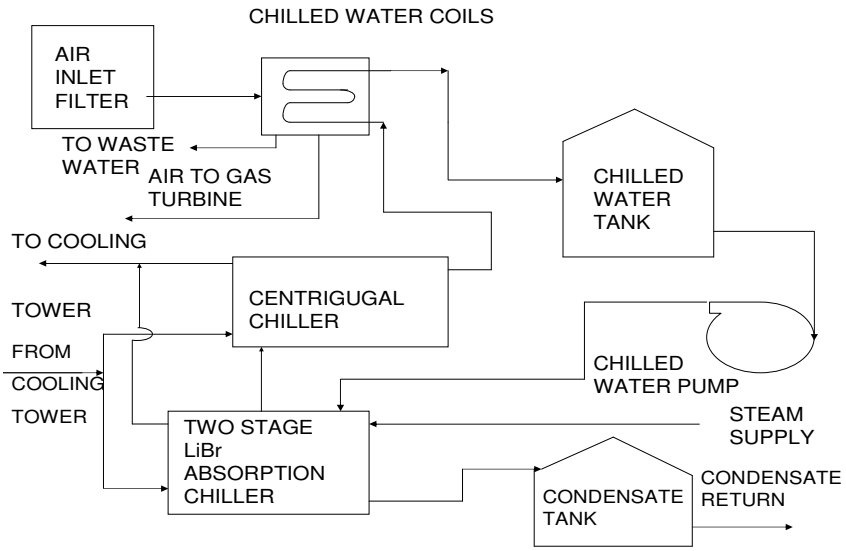

Figure 1.13 Hybrid system utilizing absorption chiller and vapour compression system

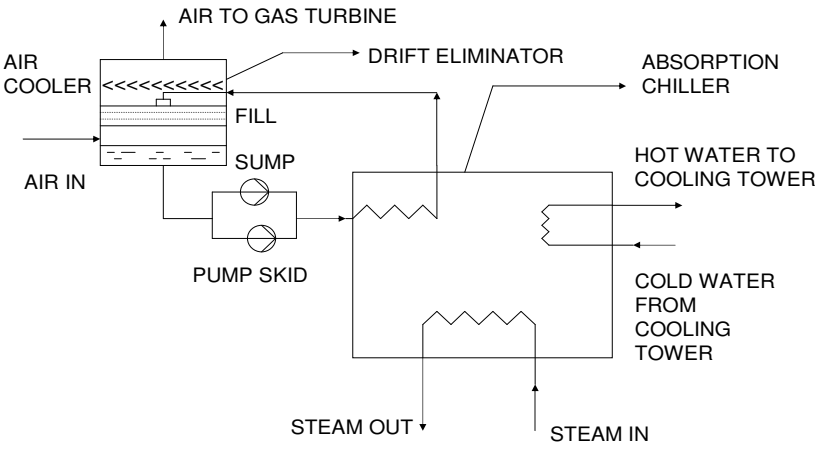

Figure 1.14 Hybrid system utilizing evaporative cooling and absorption chiller system

The direct contact air-cooler is a counter-current air-cooling system where air flows from bottom, while cold water drips down the package of the exchanger. The package works in the same manner as in conventional cooling towers. The air cools down on direct contact with the cold water produced from the absorption chiller and part of the humidity condenses directly, ensuring in this way, the lowest possible pressure drop and a high specific surface per volume. Following the air-cooler, the air flows through a droplet separator that removes water droplets from the air stream, preventing them from wetting the silencer section or the inlet duct.

The water leaving the air-cooler at a temperature of about 10°C enters the absorption chiller, where it is cooled down to 2°C. The production of cold water of 2°C requires a non-standard absorption chiller, since the refrigerant water has to be evaporated at the extremely low pressure of 7 mbar of absolute pressure (close to the triple point of water). The major improvements of the chiller used are the following:

(1) Improved heat exchange and vapour guiding systems inside the chiller due to the increased vapour volume.
(2) Improved control system to avoid freezing of the refrigerant water.
(3) Use of high performance heat exchangers in order to obtain a very high COP (COP=0.8).

The main innovation of the system is the ability to cool the suction air of the gas turbine down to 5°C, independent of ambient air temperature and humidity, this fact being a major step compared to classical air-cooling systems that cannot go much below 10°C. In order to achieve a chilled water temperature of 2°C, the control philosophy and security have been specially adapted. The risk of freezing is prevented by pollution of the evaporator with lithium bromide solution and by a low temperature switch on the chilled water circuit and the internal evaporator solution. In order to avoid risk of crystallization inside the absorption heat pump, the standard dilution sequence is implemented. In addition, the main regulation of the chiller is adjusted to minimize any regulation

instabilities leading to freezing risk. The chilled water set point is first adjusted to 6°C and then slowly to 2°C.

The system provides large flexibility since the absorption chiller can be heated by different heat sources, even by low-temperature waste heat (85-90°C). In a simple cycle gas turbine, waste heat from a heat recovery steam generator can be used to produce hot water or steam, making use of the high-energy content of the exhaust gas. In a combined cycle plant, the arrangement is similar and the heat source for the chiller can be very low-pressure bleed steam from the steam turbine (below 100°C), hot water circulated in the low-temperature feed-water preheaters (100/80 °C) or an additional low temperature coil in the boiler. The electricity consumption of the air-cooling system, including chilled water circulation pump and absorption chiller, is about 1-2 percent of the cooling capacity, depending on the size of the unit.

1.2.7 Evaporative Cooling of Pre-Compressed Air

As shown in Figure 1.15, in this gas turbine inlet air-cooling method, an electrically driven fan is used for pre-compression of the inlet air supplied to the compressor of the gas turbine, resulting in a temperature rise of the intake air. The pre-compressed air is then cooled by an evaporative cooler. Evaporative cooling of pre-compressed air is quite effective because of the higher potential of evaporative cooling for the hotter pre-compressed air stream. This method can be applied to compensate for the reduction in the air mass flow as a consequence of high ambient temperatures. This can be achieved by controlling the pressure rise of the fan, so that the air mass flow at the inlet of the compressor is maintained largely constant, regardless of the ambient condition.

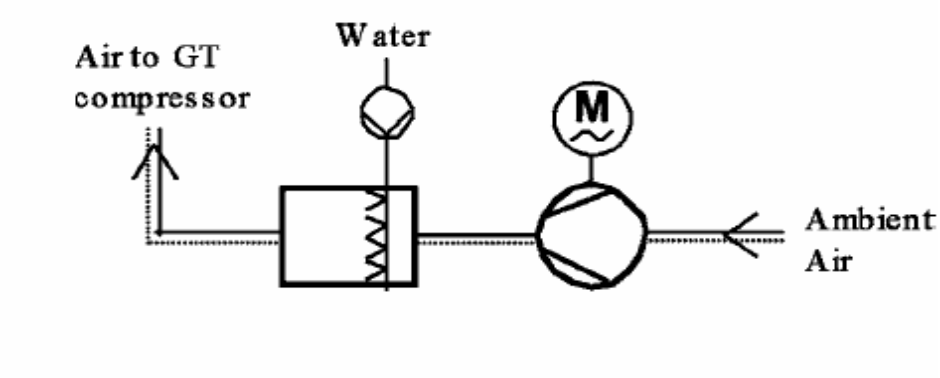

Figure 1.15 Evaporative cooling of pre-compressed air

Using this method, the gas turbine can be operated over a long period of time at its optimum operating point with regard to power output and efficiency. Also, more heat can be recovered from the exhaust gases compared to the non-cooled case. This means that, for a cogeneration system, steam production can be held constant to meet the required process steam demand. The maximum possible airflow rate is limited by the exhaust condition for the turbine and flow conditions through the compressor (surge limit).

Chapter 2
Literature Review

2.1 Introduction

Compressor intake air cooling is developing to be an important area of research in the Modern Gas Turbine Power Plants. The state of art literature survey of this area is briefly described below.

2.2 Summary of Literature Review of Different Cooling Methods

The present literature can be classified into the following categories:

a) Evaporative Cooling
b) Refrigeration Cooling
c) Hybrid System Cooling

The literature review of these systems is described below:

2.2.1 Evaporative Cooling

The evaporative cooling system is described in Chapter1, Section 1.2.1 (refer Figures 1.2 to 1.4). A summary of research work on application of evaporative cooling for gas turbine plants is given below:

Kumar and Krishna [1], investigated the improved gas turbine efficiency using spray coolers and through Alternative Regeneration Configuration. Cooling of air at compressor inlet helps in increasing the density of air flowing through the plant while alternative regeneration causes the air to enter the combustion chamber at a higher

temperature. The plant performance characteristics were examined for a set of design and operational parameters including ambient temperature, relative humidity, turbine inlet temperature and pressure ratio. At design point for reference plant (simple cycle), the efficiency was 34% whereas by using alternative regeneration and spray cooler, it increased to 47%.

Gomez *et al.* [2], presented the manufacture, test bed setup and trials carried out on a ceramic evaporative cooling system which acts as a semi-indirect cooler. The tests presented, show the system behavior for various supply air conditions. Datta *et al.* [3], fabricated and tested 8.5 ton indirect-direct evaporative cooling system and the performance of the system was compared with a computer prediction. The system's scope for use in India and Australia was analyzed.

Bejan *et al.* [4], gave the method for exergy analysis of the thermal systems. The physical and chemical exergy of various common substances was given. Al-Amiri and Zamzam [5], assessed the benefits of incorporating combustion turbine inlet air cooling systems into a reference combustion turbine plant, which was based on a simple cycle under base load mode. The main performance characteristics of both evaporative and refrigerative cooling systems were explored by examining the effect of several parameters including inlet air temperature, air flow-to-turbine output ratio, coefficient of performance and degree of hours. The impact of these parameters was presented against annual gross energy increase, average heat rate reduction, cooling load requirements and net power increase. Finally, a feasibility design chart was constructed to outline the economic returns of employing a refrigerative cooling unit against prescribed inlet air temperature values using a wide range of combustion turbine mass flow rates.

Dawoud *et al.* [6], evaluated the power requirements of several inlet air cooling techniques for gas turbine power plants in two locations: Marmul and Fahud in Oman. Fogging cooling was accompanied with 11.4% more electrical energy in comparision with evaporative cooling in both locations. The LiBr-H_2O cooling offered 40% and 55% more energy than fogging cooling at Fahud and Marmul, respectively. Applying aqua-

ammonia water and vapour compression cooling, a further annual energy production enhancement of 39% & 46% was obtained at Fahud and Marmul respectively.

Alhazmy and Najjar [7], studied the performance enhancement of gas turbine power plants using spray cooling (water spraying system and cooling coil). Spray cooler reduces the temperature of incoming air by 3-15°C enhancing the power by 1-7% and improving efficiency by 3%. Lucia *et al.* [8], presented a comparative analysis of different solutions for cooling compressor inlet air for LM600 gas turbine in a cogeneration plant operated in base load. Reference was made to two sites in northern and southern Italy whose climatic data series for modeling the variations in ambient temperature during the single day were used to account for the effects of climate in the simulation. The results confirmed evaporative cooling to be cost effective while absorption systems have a higher cost but are more versatile & powerful in base-load operation.

Bhargava and Meher-Homji [9], did a parametric analysis on the effects of inlet fogging and evaporative conditions on a wide range of existing gas turbines. Arora [10], presented a basic as well as applied thermodynamic treatment of refrigeration and air conditioning in a very comprehensive manner. A sound physical basis had been laid for obtaining fairly precise estimates of refrigeration and air-conditioning equipment.

Moran [11], presented an effective and systematic method that uses both the first and second laws of thermodynamics for the performance analysis and design of energy systems known as availability analysis. It included the use of availability equation as an important unifying concept, a thorough discussion of meaning and use of second law efficiencies, exact and appropriate methods for availability calculation and use in field of engineering economics.

Cammarata *et al*. [12], investigated an application of exergonomic theory to an air-conditioning system for optimization purposes. The thermodynamic model was stated according to recent formulations of exergy for moist air streams, while the economic

model was based on cost balance equations and real cost data for mechanical equipment. The optimum configuration was obtained through an iterative procedure aimed at the design improvement.

2.2.2 Refrigeration cooling

This system includes vapour compression and vapour absorption systems which are in use for a long time in industries. The systems are already explained in Chapter1, (Section 1.2.3. and Section 1.2.4)

Ali [13], proposed a conceptual gas turbine cycle with refrigerated air supplied to the compressor inlet, in order to increase the cycle specific net power and render it practically insensitive to seasonal temperature fluctuation. It was optimized for maximum power per kilogram per second of inducted air. Nikolaidis and Probert [14], investigated the behavior of 2-stage compound compression cycle with flash intercooling, using refrigerant R-22, by exergy method. The effects of temperature changes in condenser and evaporator, on the plant's irreversibility were determined. Haselden and Chen [15], developed and tested a steady state design simulation program for air conditioning systems using binary refrigerant mixtures. The pinch method was introduced to facilitate the refrigerant cycle simulation. Hwang [16], presented and analyzed the performance potential of a refrigeration system that is integrated with a microturbine and an absorption chiller (RMA). The assistance by the absorption chiller enhances the refrigeration cycle efficiency, especially at higher ambient temperatures, by as much as 25 and 5 % for RMA with subcooler and precooler, respectively.

Horuz and Callander [17], did an experimental investigation of the performance of a commercially available Vapour Absorption System. The cooling capacity of the plant was 10 kW and used aqua-ammonia solution as the refrigerant. The response of system to variations in chilled water inlet temperature, chilled water level in evaporator drum, chilled water flow rate and variable heat input were presented. Waked [18], carried out the Second Law Analysis for a Cogeneration Power-Absorption Cooling Plant. A

typical reference steam power plant was used to show the efficient use of fuel in producing both power and process heat to operate absorption cooling units for air-conditioning purposes.

Asdrubali *and* Grignaffini [19], obtained an experimental evaluation of a plant aimed at simulating and verifying performances of single stage H_2O-LiBr absorption machine.

Grossman and Zaltash [20], developed a computer code ABSIM for simulation of absorption systems in a flexible and modular form making it possible to investigate various cycle configurations with different working fluids. Park *et al.* [21], analyzed the performance characteristics during partial load operation and calculated energy consumption amount of H_2O/LiBr absorption chiller with a capacity of 210RT. It was concluded that when partial load is in the range of 10-40%, the reduction of the required power by 23% could be realized by decreasing cooling water inlet temperature of 1.0°C.

Lucas *et al.* [22], studied the employment of an alternative absorbent used in absorption refrigeration cycles to replace the absorbent currently employed in this kind of engines i.e., lithium bromide. The alternative system consists of absorbent (LiBr: CHO2K=2:1by mass ratio) and refrigerant (H_2O). A program was also developed to simulate the theoretical absorption cycles from empirical data. Kaita [23], developed the equations which calculate the vapour pressure, enthalpy and entropy of LiBr solutions at high temperatures. The developed equations were valid from concentrations of 40-65 wt% and also from temperatures of 40-210°C. Misra *et al*. [24], presented an application of thermoeconomic theory to the economic optimization of a single effect water/LiBr vapour absorption system aimed at minimizing its overall operation and amortization cost. Appropriate optimum design configuration was obtained by means of sequential local optimization of the system, carried out unit by unit.

Ameen [25], gave basic as well as applied thermodynamic treatment of refrigeration and air conditioning in a very comprehensive manner. The thermodynamic treatment and heat transfer formulas were also given which are helpful for the analysis of

various air conditioning equipments. Popiel and Wojtkowiak [26], presented the simple formulation of thermophysical properties of water in the temperature range of 0-150°C. The paper includes formulas for saturation pressure, density, specific enthalpy and specific entropy applicable for various air conditioning analysis purposes. Kakaras *et al.* [27], investigated the merits of integration of evaporative cooling, refrigeration cooling and evaporative cooling of pre-compressed air with two combined cycle power plants and two gas turbine plants. The calculations were performed on a yearly basis of operation and the economics from the integration of different cooling systems were calculated and compared. Cortes and Willems [28], compared the cooling techniques and systems employed for power generation gas turbine inlet air applications. The comparision between fogging and media based evaporative cooling and chilling (refrigeration cycle) in various inlet ambient conditions was done.

Talbi and Agnew [29], carried out exergy analysis on a single-effect absorption refrigeration cycle with lithium-bromide-water as the working fluid pair. Numerical results for the cycle were tabulated. A design procedure was applied to a lithium-bromide absorption cycle and an optimization procedure that consists of determining the enthalpy, entropy, temperature, mass flow rate and heat rate in each component, and coefficient of performance was calculated. Kizilkan *et al.* [30], applied the thermoeconomic optimization technique to a LiBr absorption refrigeration system. Various components of the system such as condenser, evaporator, generator and absorber heat exchangers were optimized and heat exchanger areas with corresponding optimum operating temperatures were determined.

Florides *et al.* [31], presented the modeling, simulation and total equivalent warming impact of a domestic-size absorption solar cooling system. The system was modeled with the TRNSYS simulation program using appropriate equations predicting the performance of the unit. Joudi and Lafta [32], developed a steady state computer simulation model to predict the performance of an absorption refrigeration system using LiBr-water as a working pair. A computer program was developed to simulate the effect of various operating conditions on the performance of the individual components of the

simulated system. A new model was introduced for representing the absorber. The performance of absorber, generator, condenser and evaporator were simulated independently. The whole system was then simulated as a working absorption cycle under various operating conditions.

Misra *et al.* [33], applied the thermoeconomic concept to the optimization of a double-effect H_2O-LiBr vapour absorption refrigeration system, aimed at minimizing its overall product cost. A simplified cost minimization methodology based on the thermoeconomic concept was applied to calculate the economic costs of all the internal flows and products of the system by formulating the thermoeconomic cost balances. The sensitivity analysis showed that the changes in optimal values of the decision variables are negligible with changes in the fuel cost. Xu *et al.* [34], presented an advanced energy storage system using aqueous lithium bromide as working fluid. The working principle and flow of the variable mass energy transformation and storage (VMETS) system were introduced and the system dynamic models were developed. Xu *et al.* [35], numerically simulated the advanced energy storage system using LiBr-water as the working fluid, to investigate the system dynamic characteristics and performances when it works to provide combined air-conditioning and hot water supplying for a hotel located in China. The simulation results included the temperature and concentration of the working fluid, the mass and energy in the storage tanks, the compressor intake mass or volume flow rate, discharge pressure, compression ratio, power and consumption work, the heat loads of heat exchanger devices in the system.

Tozer and James [36], derived the thermodynamic absorption cycle performance and temperature formulae. Ideal absorption cycle was demonstrated as the combination of a Carnot driving cycle with a Reverse Carnot cooling cycle. Performance and temperature relations of double, triple and multistage cycles were derived. Validation of the fundamental thermodynamics of absorption cycles was presented by applying an exergy analysis. Valladares *et al.* [37], carried out a detailed one-dimensional steady and transient numerical simulation of the thermal and fluid-dynamic behaviour of double-pipe heat exchangers. The governing equations (continuity, momentum and energy) inside the

internal tube and the annulus, together with the energy equation in the internal tube wall, external tube wall and insulation were solved iteratively in a segregated manner. Different numerical aspects and comparisions with analytical and experimental results were presented.

Tozer *et al.* [38], described the use of the T-s diagram of water extended with additional curves to represent real and ideal water/LiBr absorption cycles. An explanation was provided on several methods available, including details of the thermodynamic justification of the method used, to construct the extended diagrams. Extended T-s diagram was provided with the representation of a real single-effect water/LiBr absorption refrigeration cycle.

2.2.3 Hybrid system cooling

Ondryas *et al*. [39], investigated the gas turbine power augmentation in a cogeneration plant using inlet air chilling by the combined application of centrifugal and absorption chilling systems. The system was sized for one-half of the cooling by absorption and the other by centrifugal chilling. A temperature reduction of 23°C was observed. Application of the hybrid system resulted in lower chilled water temperatures and less pumping and piping costs. Kakaras *et al.* [40], simulated the results for two test cases: a simple cycle gas turbine and a combined cycle plant. First, the effect of ambient air temperature variation on the power output and efficiency was determined, demonstrating the large penalty in the plant's performance for higher ambient temperatures. Further, the results from the integration of an evaporative cooler and of absorption chilling system were presented, demonstrating the gain in power output and efficiency that can be achieved. The hybrid system demonstrated a higher gain in power output and efficiency than evaporative cooling for a simple gas turbine, independent of ambient air temperature.

2.3 Conclusions

By the study of present literature following conclusions can be drawn:

a) Evaporative cooling system is the cheapest cooling system in use today.

b) Gain in output is approximately 5% by the use of evaporative cooling system.

c) Vapour compression and vapour absorption system produce more degree of cooling than evaporative cooling system.

d) Vapour compression and vapour absorption system are more expensive than evaporative cooling system.

e) Performance of the selected system is largely affected by the local weather patterns.

f) Hybrid systems offer a greater degree of cooling and therefore power output and efficiency of the gas turbine plant is higher.

2.4 Scope of the work

From the literature survey of work done by different people on the compressor intake air-cooling, it is very clear that lot of scope is lying in analyzing the methods of air-cooling. Evaporative cooling and absorption chiller system are the good choice for economical and efficiency purpose. In the present work, energy and second law analysis of Water/LiBr vapour absorption refrigeration system has been investigated by the exergy method.

Chapter 3
Formulation of VAR System

3.1 Description of Water/LiBr VAR system

The absorption chiller system is already been described in Chapter 1, (Section 1.2.4). The simplified schematic of the system for analysis is shown in Figure 3.1

The water (refrigerant) is boiled off from the steam coils in generator (process 3-7) and high-pressure water vapour is condensed over cooling coils in condenser (process 7-8). The condensate is supplied through an expansion valve (process 8-9) into evaporator where it gets heat from the circulating water and is converted into low-pressure water vapour (process 9-10) which is then fed into absorber. The weak concentration solution of water in LiBr remaining in the generator is also fed back to the absorber (process 4-5) through the heat exchanger and throttling valve (process 5-6). The above two streams mix and form a strong solution which is fed ultimately through the solution pump to generator (process 1-3) after getting heated in the heat exchanger. The solution pump is used to raise the solution to a higher pressure (process 2-3) in generator from a lower pressure maintained in absorber. Air heat exchanger is used to reduce the temperature of the inlet air by giving the energy to the chilled water coming from the absorption system, which serves as the cooling load for VAR system. The system gains the energy from the hot water circulating in generator coils (process 17-18). Heat rejected by condenser and absorber is carried by the cooling water (process 11 to 16) which ultimately rejects the heat in cooling tower.

The enthalpy-concentration and equilibrium chart for the system is shown in Figure 3.2 and Figure 3.3 respectively.

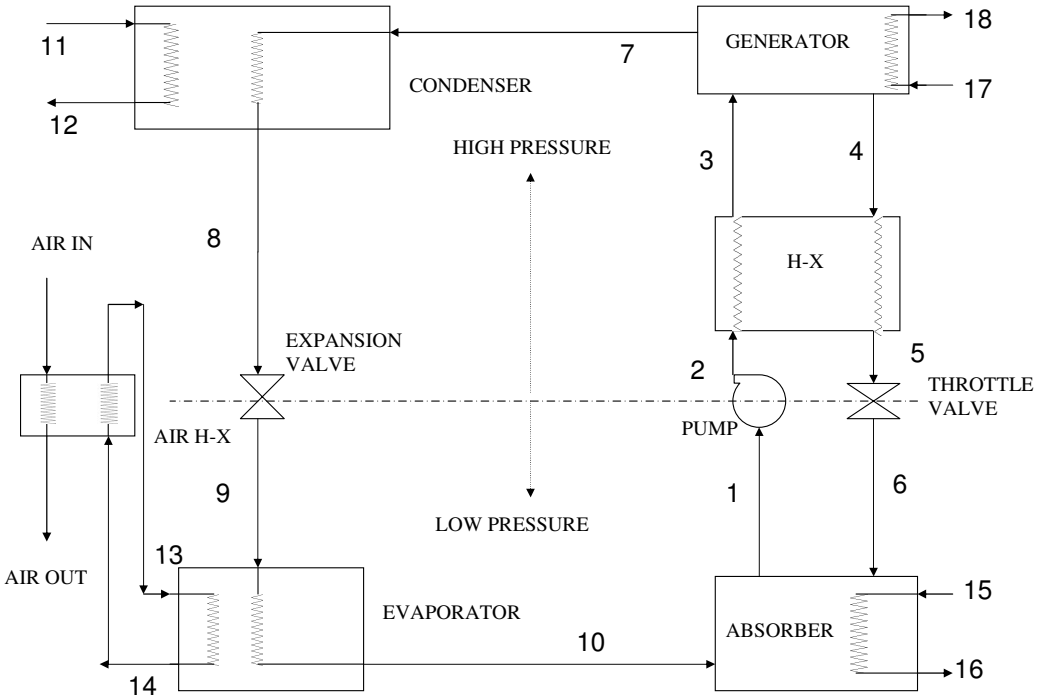

1-Strong water concentration LiBr solution leaving absorber

2-Strong water concentration LiBr solution entering heat exchanger

3-Strong water concentration LiBr solution leaving heat exchanger

4-Weak water concentration LiBr solution leaving generator

5-Weak water concentration LiBr solution leaving heat exchanger

6- Weak water concentration LiBr solution entering absorber

7-High pressure water vapour

8-High pressure water

9-Low pressure water

10-Low pressure water vapour

11- Cooling water in

12-Cooling water out

13-Inlet chilled water

14-Outlet chilled water

15-Cooling water in

16- Cooling water out

17- Hot water in

18- Hot water out

Figure 3.1 Water/ LiBr Vapour absorption refrigeration system

.

Figure 3.2 Equilibrium diagram for Water/LiBr vapour absorption refrigeration system

Figure 3.3 Specific enthalpy (h) vs concentration (x) diagram for Water/LiBr vapour absorption refrigeration system

3.2 Formulation of Water/LiBr VAR system

3.2.1 Energy analysis

For the thermodynamic analysis of vapour absorption refrigeration system, the energy and mass balance equations of the various components are given below.

Air Heat Exchanger

The heat exchange in air heat exchanger is given by

$$Q_{ex} = (V/v_{air,\,in})\, C_{pa,\,in}\, T_{air,\,in} - (V/v_{air,\,out})\, C_{pa,\,out}\, T_{air,\,out} \qquad (3.1)$$

where,

Q_{ex} = Heat exchanged in the air heat exchanger in kW.

V = Volumetric air flow rate in cu.m/s.

$v_{air,\,in}$ = Specific volume of inlet air in cu.m/kg.

$v_{air,\,out}$ = Specific volume of exit air in cu.m/kg.

$C_{pa,\,in}$ = Specific heat of inlet air in kJ/kgK.

$C_{pa,\,out}$ = Specific heat of exit air in kJ/kgK.

$T_{air,\,in}$ = Inlet air temperature in K.

$T_{air,\,out}$ = Exit air temperature in K.

Evaporator

The energy balance in evaporator is given by

$$Q_e = m_{13} (h_{13} - h_{14}) \quad (3.2)$$

where,

Q_e = Cooling load in evaporator in kW.

m_{13} = Mass flow rate of chilled water to evaporator in kg/s.

h_{13} = Specific enthalpy of inlet chilled water in evaporator in kJ/kg.

h_{14} = Specific enthalpy of outlet chilled water in evaporator in kJ/kg.

also, $$Q_e = Q_{ex} \quad (3.3)$$

$$= m_9 h_{fg,\,e} \quad (3.4)$$

where,

m_9 = Mass flow rate of refrigerant water entering evaporator in kg/s.

$h_{fg,\,e}$ = Latent heat of vaporization of water at evaporator temperature (T_{ce}) in kJ/kg.

From equation (3.4)

$$m_9 = Q_e / h_{fg,\,e} \quad (3.5)$$

$$m_{10} = m_9 \quad (3.6)$$

where,

m_{10} = Mass flow rate of low pressure water vapour from evaporator in kg/s.

also,

$$m_{14} = m_{13} \quad (3.7)$$

where,

m_{14} = Mass flow rate of chilled water from evaporator in kg/s.

Expansion valve

The energy balance equation for expansion valve is given by

$$h_9 = h_8 \quad (3.8)$$

where,

h_8 = Specific enthalpy of water at condenser temperature (T_{hc}) in kJ/kg.

also,

$$m_8 = m_9 \quad (3.9)$$

where,

m_8 = Mass flow rate of refrigerant water leaving condenser in kg/s.

Condenser

The energy balance in condenser is given by

$$Q_c = m_7 h_7 - m_8 h_8 \quad (3.10)$$

where,

Q_c = Heat rejected in condenser in kW.

m_7 = Mass flow rate of high pressure water vapour leaving generator at generator temperature (T_g) and pressure (P_g) in kg/s.

h_7 = Specific enthalpy of high-pressure water vapour in kJ/kg.

also,

$$Q_c = m_{11} (h_{12} - h_{11}) \quad (3.11)$$

where,

m_{11} = Mass flow rate of cooling water entering condenser in kg/s.

h_{12} = Specific enthalpy of cooling water leaving condenser in kJ/kg.

h_{11} = Specific enthalpy of cooling water entering condenser in kJ/kg.

From equation (3.11)

$$m_{11} = Q_c / (h_{12} - h_{11}) \quad (3.12)$$

and,

$$m_{12} = m_{11} \tag{3.13}$$

also,

$$m_7 = m_8 \tag{3.14}$$

Solution heat exchanger

The temperature of strong water concentration LiBr solution leaving solution heat exchanger is given by

$$T_3 = \varepsilon (T_g - T_a) + T_a \tag{3.15}$$

where,

T_a= Temperature of absorber in K.

T_g= Temperature of generator in K.

ε = Effectiveness of solution heat exchanger.

and, energy balance in solution heat exchanger is

$$Q_{hx} = m_3h_3 - m_2h_2 \tag{3.16}$$

$$= m_4h_4 - m_5h_5 \tag{3.17}$$

where,

Q_{hx} = Heat exchange in solution heat exchanger in kW.

m_3 = Mass flow rate of strong water concentration LiBr solution leaving solution heat exchanger in kg/s.

h_3 = Specific enthalpy of strong water concentration LiBr solution leaving solution heat exchanger at temperature (T_3) in kJ/kg.

m_2 = Mass flow rate of strong water concentration LiBr solution entering solution heat exchanger in kg/s.

h_2 = Specific enthalpy of strong water concentration LiBr solution entering solution heat exchanger in kJ/kg.

m_4 = Mass flow rate of weak water concentration LiBr solution entering solution heat exchanger in kg/s.

h_4 = Specific enthalpy of weak water concentration LiBr solution entering solution heat exchanger at temperature (T_g) in kg/s.

m_5 = Mass flow rate of weak water concentration LiBr solution leaving solution heat exchanger in kg/s.

h_5 = Specific enthalpy of weak water concentration LiBr solution leaving solution heat exchanger in kJ/kg.

From equation (3.17)

$$h_5 = h_4 - Q_{hx} / m_4 \qquad (3.18)$$

since,

$$m_2 = m_3 \tag{3.19}$$

$$m_5 = m_4 \tag{3.20}$$

Generator

The energy balance for generator is

$$Q_g = m_4h_4 + m_7h_7 - m_3h_3 \tag{3.21}$$

where,

Q_g = Heat load in generator in kW.

also, from external means, low grade energy (hot water) supplied to generator is

$$Q_g = m_{17} (h_{17} - h_{18}) \tag{3.22}$$

where,

m_{17} = Mass flow rate of hot water entering generator coils in kg/s.

h_{17} = Specific enthalpy of hot water entering generator in kJ/kg.

h_{18} = Specific enthalpy of hot water leaving generator in kg/s.

From equation (3.22)

$$m_{17} = Q_g / (h_{17} - h_{18}) \tag{3.23}$$

also,

$$m_{18} = m_{17} \tag{3.24}$$

$$m_3 = m_4 + m_7 \tag{3.25}$$

$$m_3 x_3 = m_4 x_4 \tag{3.26}$$

where,

x_3 = Concentration in weight percent of LiBr in the strong water concentration LiBr solution.

x_4 = Concentration in weight percent of LiBr in the weak water concentration LiBr solution.

Absorber

The heat balance in absorber is represented by

$$Q_a = m_{10}h_{10} + m_6h_6 - m_1h_1 \tag{3.27}$$

where,

Q_a = Heat rejected in absorber in kW.

h_{10} = Specific enthalpy of low pressure saturated water vapour at temperature (T_{ce}) in kJ/kg.

h_6 = Specific enthalpy of weak water concentration LiBr solution entering absorber in kJ/kg.

h_1 = Specific enthalpy of strong water concentration LiBr solution leaving absorber at temperature (T_a) and concentration (x_2) in kJ/kg.

m_6 = Mass flow rate of weak water concentration LiBr solution entering absorber in kg/s.

m_1= Mass flow rate of strong water concentration LiBr solution leaving absorber kg/s.

also,

$$Q_a = m_{15} (h_{16} - h_{15}) \quad (3.28)$$

where,

m_{15} = Mass flow rate of cooling water in absorber in kg/s.

h_{16} = Specific enthalpy of cooling water leaving absorber in kJ/kg.

h_{15} = Specific enthalpy of cooling water entering absorber in kJ/kg.

From equation (3.28)

$$m_{15} = Q_a / (h_{16} - h_{15}) \quad (3.29)$$

and,

$$m_{16} = m_{15} \quad (3.30)$$

$$m_1 = m_6 + m_{10} \quad (3.31)$$

Pump

Work supplied to the pump is given by

$$W_{pump} = m_1 (P_g - P_a) / \rho \quad (3.32)$$

where,

W_{pump} = Power consumption of pump in kW.

P_g = Pressure in generator in kPa.

P_a = Pressure in absorber in kPa.

ρ = Density of Water/LiBr solution (2238.5 kg/cu.m).

and,

$$m_2 = m_1 \quad (3.33)$$

Throttle valve

For a throttling process

$$h_5 = h_6 \quad (3.34)$$

$$m_5 = m_6 \quad (3.35)$$

The rich refrigerant concentration solution circulation ratio is given by

$$f = x_4 / (x_4 - x_3) \quad (3.36)$$

Coefficient of performance of the system is given as

$$COP = Q_e / (Q_g + W_{pump}) \quad (3.37)$$

3.2.2 Second law analysis

Second law analysis is a relatively new concept, which has been used for understanding the irreversible nature of real thermal processes and defining the maximum available energy. The second law analysis is based on the concept of exergy, which can be defined as a measure of work potential or quality of different forms of energy relative to the environmental conditions. In other words, exergy can be defined as the maximum theoretical work, derivable by the interaction of an energy resource with the environment.

Exergy analysis applied to a system describes all losses both in the various components of the system and in the whole system. With the help of this analysis, the magnitude of these losses or irreversibilities and their order of importance can be understood. With the use of irreversibility, which is a measure of process imperfection, the optimum operating conditions can be easily determined. The advantage of exergy analysis based on thermoeconomic optimization is that the different elements of the system could be optimized independently. It is possible to say that exergy analysis can indicate the possibilities of thermodynamic improvement of the process under consideration.

In the absence of magnetic, electrical, nuclear, surface tension effects, and considering the system is at rest relative to the environment, the total exergy of a system can be divided into two components: physical exergy (E^{Ph}) and chemical exergy (E^{Ch}).

$$\text{i.e., } E = E^{Ph} + E^{Ch} \quad (3.38)$$

The physical exergy component is associated with work obtainable in bringing a stream of matter from initial state to a state that is in thermal and mechanical equilibrium with the environment. Mathematically, physical exergy is expressed as

$$E^{Ph} = m\,[(h - h_0) - T_0\,(s - s_0)] \tag{3.39}$$

where,

h = Specific enthalpy of fluid in kJ/kg.

s = Specific entropy of fluid in kJ/kgK.

h_0 = Specific enthalpy of water at reference point (298.15 K) in kJ/kg.

s_0 = Specific entropy of water at reference point in kJ/kgK.

T_0 = Reference point temperature (298.15 K).

The chemical exergy component is associated with work obtainable in bringing a stream of matter from state that is in thermal and mechanical equilibrium with the environment to a state of that stream of matter, which is in the most stable configuration in equilibrium with the environment. As there is no chemical reaction in the components of vapour absorption refrigeration system, including the generator and absorber, the chemical state of the absorbent remains the same throughout the absorber circuit. Therefore, the change in chemical exergy of the water is only considered, while that of LiBr is neglected in the analysis [24]. Mathematically, chemical exergy of the flows in water (refrigerant) can be expressed as

$$E^{Ch} = m\,[\{1 - (x/100)\}/\,M_{H2O}]\,\dot{e}_{Ch,\,H2O} \tag{3.40}$$

where,

m = Mass flow rate of fluid in kg/s.

x = Concentration of LiBr in fluid stream in weight percent.

M_{H2O} = Molecular mass of water.

$\dot{e}_{Ch, H2O}$= Standard specific chemical exergy of water in liquid state [4] in kW/kmol at temperature 298.15 K and pressure 101.325 kPa.

A detailed exergy analysis includes calculating exergy destruction (E_D), exergy loss (E_L), exergetic efficiency (η_{ex}), exergy destruction ratio (Y_D), exergy loss ratio or efficiency defect (Y_L) in each component of the system along with the overall system. The exergy destruction is the amount of exergy that is lost to the environment and cannot be used anywhere. The exergy loss represents the amount of exergy that is transferred from the analyzed system to some other system (s), e.g. cooling water loss. Overall, for a control volume the steady-state exergy balance can be expressed as

$$\sum E_{in} - \sum E_{out} - Q(1 - T_0 / T) - W - E_D = 0 \quad (3.41)$$

where,

E_{in} = Exergy entering in the system in kW.

E_{out} = Exergy leaving the system in kW.

Q = Heat loss in the system in kW.

T = Temperature at which the heat loss occurs in K.

W = Work done by the system in kW.

The exergy destruction (or irreversibility) in a component is calculated from the exergy balance as

$$E_{D,\,k} = E_{F,\,k} - E_{P,\,k} - E_{L,\,k} \tag{3.42}$$

where,

$E_{F,\,k}$ = Fuel exergy in k_{th} component of the system in kW.

$E_{P,\,k}$ = Product exergy in k_{th} component of the system in kW.

$E_{L,\,k}$ = Exergy loss in k_{th} component of the system in kW.

The exergetic efficiency of the components and the overall system shows what percentage of the fuel exergy can be found in the product exergy, i.e.,

$$\eta_{ex,\,k} = E_{P,\,k} / E_{F,\,k} \tag{3.43}$$

The exergy destruction ratio compares the exergy destruction in the k_{th} component with the total exergy supplied to the system, i.e.,

$$Y_D = E_{D,\,k} / E_{F,\,overall} \tag{3.44}$$

The exergy loss ratio compares the exergy loss in the k_{th} component with the total exergy supplied to the system, i.e.,

$$Y_L = E_{L,\,k} / E_{F,\,overall} \tag{3.45}$$

The 'Fuel – Product – Loss' and exergetic terms' definition for the various components of vapour absorption system (refer Figure 3.1) is shown in Table 3.1 to 3.4.

Table 3.1 Fuel – Product – Loss definitions of the Water/LiBr vapour absorption refrigeration system

Systems	Fuels	Products	Losses
Generator	$E_{17} - E_{18}$	$E_7 + E_4 - E_3$	-
Evaporator assembly	$E_5 + E_7 - E_1$	$E_{14} - E_{13}$	$(E_{16} - E_{15}) + (E_{12} - E_{11})$
Solution pump	W_{Pump}	$E_2 - E_1$	-
Solution heat exchanger	$E_4 - E_5$	$E_3 - E_2$	-
Overall system	$E_{17} - E_{18}$	$E_{14} - E_{13}$	$(E_{16} - E_{15}) + (E_{12} - E_{11})$

Since, the product cannot be defined readily for the heat dissipative devices, i.e., condenser, absorber and two throttling devices [4], all these components are considered as a single virtual component together with the components they serve. Furthermore, the analysis is also done for these individual components (Table 3.2) which is debatable but this doesn't affect the main analysis in anyway. In the case of exergy loss streams corresponding to the heat rejection to cooling medium, either it is included in the fuel term of the component and is charged to overall system. In the second option, the exergy loss streams should be shown separately with the overall system. In this work, second option is considered for its simplicity.

Definition of exergetic terms in reference to Vapour Absorption Refrigeration system components and evaporator assembly are given in Table 3.3 and Table 3.4 respectively.

Table 3.2 Fuel – Product – Loss definitions of the subsystems of evaporator assembly

Subsystems	Fuels	Products	Losses
Combined evaporator and expansion valve	$E_8 - E_{10}$	$E_{14} - E_{13}$	-
Combined absorber and throttle valve	$E_{10} + E_5$	E_1	$(E_{16} - E_{15})$
Condenser	E_7	E_8	$(E_{12} - E_{11})$

[Following the methodology described by Bejan *et al.* [4], expansion valve is considered with evaporator. Similarly, throttle valve is included with absorber].

Table 3.3 Definition of exergetic terms for vapour absorption system components' assembly

Systems	E_D	$\eta_{ex,k}$	E_L	Y_D	Y_L
Generator	$(E_{17} - E_{18}) - (E_7 + E_4 - E_3)$	$(E_7 + E_4 - E_3) / (E_{17} - E_{18})$	-	$[(E_{17} - E_{18}) - (E_7 + E_4 - E_3)] / (E_{17} - E_{18})$	-
Evaporator assembly	$(E_5 + E_7 - E_1) - (E_{14} - E_{13}) - (E_{16} - E_{15}) - (E_{12} - E_{11})$	$(E_{14} - E_{13}) / (E_5 + E_7 - E_1)$	$(E_{16} - E_{15}) + (E_{12} - E_{11})$	$[(E_5 + E_7 - E_1) - (E_{14} - E_{13}) - (E_{16} - E_{15}) - (E_{12} - E_{11})] / (E_{17} - E_{18})$	$[(E_{16} - E_{15}) + (E_{12} - E_{11})] / (E_{17} - E_{18})$
Solution pump	$W_{Pump} - (E_2 - E_1)$	$(E_2 - E_1) / W_{Pump}$	-	$[W_{Pump} - (E_2 - E_1)] / (E_{17} - E_{18})$	-
Solution heat exchanger	$(E_4 - E_5) - (E_3 - E_2)$	$(E_3 - E_2) / (E_4 - E_5)$	-	$[(E_4 - E_5) - (E_3 - E_2)] / (E_{17} - E_{18})$	-
Overall system	$(E_{17} - E_{18}) - (E_{14} - E_{13}) - (E_{16} - E_{15}) - (E_{12} - E_{11})$	$(E_{14} - E_{13}) / (E_{17} - E_{18})$	$(E_{16} - E_{15}) + (E_{12} - E_{11})$	$[(E_{17} - E_{18}) - (E_{14} - E_{13}) - (E_{16} - E_{15}) - (E_{12} - E_{11})] / (E_{17} - E_{18})$	$[(E_{16} - E_{15}) + (E_{12} - E_{11})] / (E_{17} - E_{18})$

Table 3.4 Definition of exergetic terms for components of evaporator assembly

Subsystems	E_D	$\eta_{ex,k}$	E_L	Y_D	Y_L
Combined evaporator and expansion valve	$(E_8 - E_{10}) - (E_{14} - E_{13})$	$(E_{14} - E_{13}) / (E_8 - E_{10})$	-	$[(E_8 - E_{10}) - (E_{14} - E_{13})] / (E_{17} - E_{18})$	-
Combined absorber and throttle valve	$(E_{10} + E_5) - E_1 - (E_{16} - E_{15})$	$E_1 / (E_{10} + E_5)$	$(E_{16} - E_{15})$	$[(E_{10} + E_5) - (E_1) - (E_{16} - E_{15})] / (E_{17} - E_{18})$	$[(E_{16} - E_{15})] / (E_{17} - E_{18})$
Condenser	$(E_7 - E_8) - (E_{12} - E_{11})$	E_8 / E_7	$(E_{12} - E_{11})$	$[(E_7 - E_8) - (E_{12} - E_{11})] / (E_{17} - E_{18})$	$[(E_{12} - E_{11})] / (E_{17} - E_{18})$ -

The above exergy analysis formulation are performed on each component of the vapour absorption refrigeration system. The final form of the formulation for exergy destruction of the components are given below.

Exergy destruction in the generator is represented by

$$E_{D,\,g} = T_0 [m_4 s_4 - m_3 s_3 - m_{17} (s_{17} - s_{18}) + m_7 s_7] + [\{m_3 [(1- x_3 / 100) / M_{H2O}] \dot{e}_{Ch,\,H2O}\} - \{m_4 [(1- x_4 /100) / M_{H2O}] \dot{e}_{Ch,\,H2O}\} - \{m_7 (1/ M_{H2O}) \dot{e}_{Ch,\,H2O}\}] \quad (3.46)$$

where,

s_4 = Specific entropy of weak water concentration LiBr solution entering solution heat exchanger at temperature (T_g) in kJ/kgK.

s_3 = Specific entropy of strong water concentration LiBr solution leaving solution heat exchanger at temperature (T_3) in kJ/kgK.

s_7 = Specific entropy of high pressure water vapour leaving generator at temperature (T_g) in kJ/kgK.

s_{17} = Specific entropy of hot water entering generator coils in kJ/kgK.

s_{18} = Specific entropy of hot water leaving generator coils in kJ/kgK.

x_3 = Concentration of LiBr in strong water concentration solution in weight percent.

x_4 = Concentration of LiBr in weak water concentration solution in weight percent.

Exergy destruction in the evaporator assembly is described by

$$E_{D,\,ea} = T_0 [m_1 s_1 - m_5 s_5 - m_7 s_7 + m_{13} (s_{14} - s_{13}) + m_{15} (s_{16} - s_{15}) + m_{11} (s_{12} - s_{11})] + [\{m_5 [(1- x_4 /100) / M_{H2O}] \dot{e}_{Ch,\,H2O}\} - \{m_1 [(1- x_3 /100) / M_{H2O}] \dot{e}_{Ch,\,H2O}\} + \{m_7 [1 / M_{H2O}] \dot{e}_{Ch,\,H2O}\}] \quad (3.47)$$

where,

s_1 = Specific entropy of strong water concentration LiBr solution leaving absorber at temperature (T_a) in kJ/kgK.

s_5 = Specific entropy of weak water concentration LiBr solution leaving solution heat exchanger in kJ/kgK.

s_{11} = Specific entropy of cooling water entering condenser in kJ/ kg K.

s_{12} = Specific entropy of cooling water leaving condenser in kJ/ kg K.

s_{13} = Specific entropy of inlet chilled water in evaporator in kJ/ kg K.

s_{14} = Specific entropy of outlet chilled water from evaporator in kJ/ kg K.

s_{15} = Specific entropy of cooling water entering absorber in kJ/ kg K.

s_{16} = Specific entropy of cooling water leaving absorber in kJ/ kg K.

Exergy destruction in the solution heat exchanger is

$$E_{D,\,hx} = T_0 [m_3 s_3 - m_2 s_2 - m_4 s_4 + m_5 s_5] + [\{m_4 [(1- x_4 /100) / M_{H2O}] \dot{e}_{Ch,\,H2O}\} - \{m_3 [(1- x_3 /100) / M_{H2O}] \dot{e}_{Ch,\,H2O}\} + \{m_2 [(1- x_3 /100) / M_{H2O}] \dot{e}_{Ch,\,H2O}\} - \{m_5 [(1- x_4 /100) / M_{H2O}] \dot{e}_{Ch,\,H2O}\} \quad (3.48)$$

where,

s_2 = Specific entropy of strong water concentration LiBr solution entering solution heat exchanger in kJ/kgK.

Exergy destruction in the overall system,

$$E_{D,\,overall} = T_0 [m_{13} (s_{14} - s_{13}) + m_{15} (s_{16} - s_{15}) + m_{11} (s_{12} - s_{11}) - m_{17} (s_{17} - s_{18})] \quad (3.49)$$

Exergy destruction in combined evaporator and expansion valve,

$$E_{D,\,e} = T_0 [m_8 (s_{10} - s_8) - m_{13} (s_{13} - s_{14})] + [\{m_8 [1 / M_{H2O}] \dot{e}_{Ch,\,H2O}\} - \{m_{10} [1 / M_{H2O}] \dot{e}_{Ch,\,H2O}\}] \quad (3.50)$$

where,

s_{10} = Specific entropy of saturated water vapour leaving evaporator at temperature (T_{ce}) in kJ/ kg K.

s_8 = Specific entropy of refrigerant water leaving condenser at temperature (T_{hc}) in kJ/ kg K.

Exergy destruction in combined absorber and throttle valve is

$$E_{D,\,a} = T_0 [m_1 s_1 - m_5 s_5 - m_{10} s_{10} - m_{15} (s_{15} - s_{16})] + [\{m_5 [(1 - x_4 /100) / M_{H2O}] \dot{e}_{Ch,\,H2O}\} + \{m_{10} [1 / M_{H2O}] \dot{e}_{Ch,\,H2O}\} - \{m_1 [(1 - x_3 /100) / M_{H2O}] \dot{e}_{Ch,\,H2O}\}] \quad (3.51)$$

Exergy destruction in the condenser is

$$E_{D,\,c} = T_0 [m_7 (s_8 - s_7) - m_{11} (s_{11} - s_{12})] + [\{m_7 [1 / M_{H2O}] \dot{e}_{Ch,\,H2O}\} - \{m_8 [1 / M_{H2O}] \dot{e}_{Ch,\,H2O}\}] \quad (3.52)$$

In the above formulation, since the total exergy leaving the solution pump (E_2) is the sum of total exergy entering (E_1) and power consumed by the pump (W_{pump}), exergy destruction in the solution pump is zero.

Coefficient of structural bonds (CSB)

The change of local irreversibility rates and exergy fluxes in relation to the overall plant's irreversibility rate is effectively expressed as Coefficient of Structural Bonds, which is defined as

$$\sigma_k = (\delta E_{D,\,overall}) / (\delta E_{D,\,k})_{xi} \quad (3.53)$$

where,

$\delta E_{D,\,overall}$ = Change in total plant's irreversibility rate in kW.

$\delta E_{D,\,k}$ = Change in component's irreversibility rate in kW.

xi = Variable, generally temperature of the component.

On a graph between total plant's irreversibility rate and component's irreversibility rate, Coefficient of Structural Bonds is represented by the average slope of the line.

3.2.3 Development of subroutines for system parameter calculations

As shown in Figure 3.4 and Figure 3.5, the subroutine calculation is done to predict various state combinations of the system components and perform system calculations. Subroutine 1 predicts the rich refrigerant concentration solution circulation ratio (f) for fixed values of absorber, evaporator, condenser and generator temperatures. Subroutine 2 predicts the variation of generator temperature (T_g) with the variation of condenser and absorber temperatures (T_{hc} and T_a) respectively, for a constant value of evaporator temperature (T_{ce}) and rich refrigerant concentration solution circulation ratio (f). Subroutine 3 predicts the variation of evaporator temperature with the variation of condenser and absorber temperatures respectively, for a constant value of generator temperature and rich refrigerant concentration solution circulation ratio. The heat gain in generator is given by

$$Q_g = m_{17}\, C_{ps}\, (T_{17} - T_{18}) \tag{3.54}$$

where,

C_{ps} = Specific heat of water in kJ/kgK.

T_{17} = Temperature of hot water entering generator coils in K.

T_{18} = Temperature of hot water leaving generator coils in K.

Heat loss in absorber is given by

$$Q_a = m_{15}\, C_{ps}\, (T_{16} - T_{15}) \tag{3.55}$$

where,

T_{16} = Temperature of cooling water leaving absorber in K.

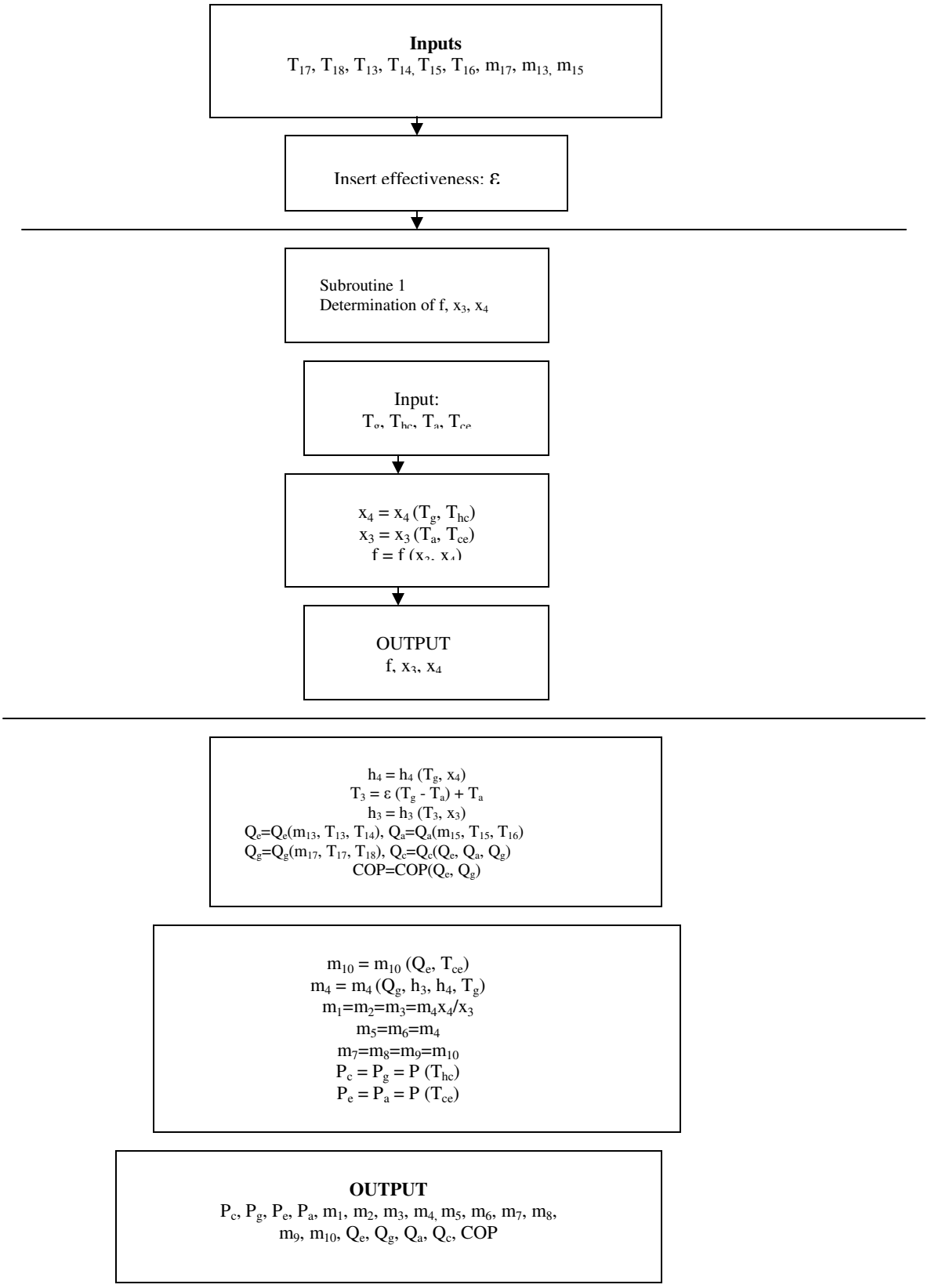

Figure 3.4 Flow Chart for system calculation

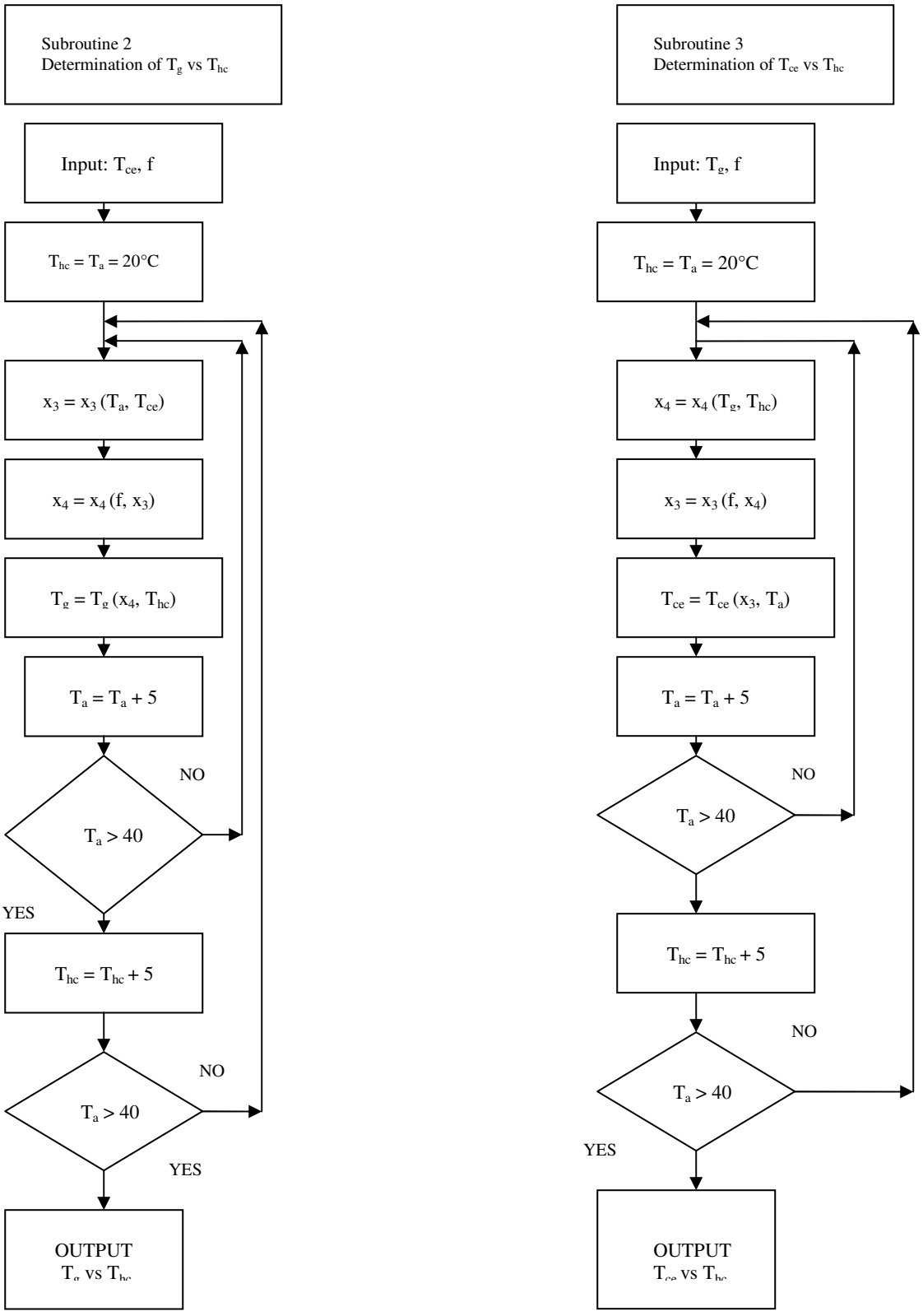

Figure 3.5 Flow charts for subroutine 2 and 3

T_{15} = Temperature of cooling water entering absorber in K.

Cooling load in evaporator is given by

$$Q_e = m_{13} C_{ps} (T_{13} - T_{14}) \quad (3.56)$$

where,

T_{13} = Temperature of inlet chilled water in evaporator in K.

T_{14} = Temperature of outlet chilled water from evaporator in K.

Heat loss in condenser is given by

$$Q_c = (Q_e + Q_g) - Q_a \quad (3.57)$$

Temperature (T_3) and coefficient of performance (COP) are given by the equations (3.15) and (3.37) respectively. Different mass flow rates except (m_4) are given by equations (3.5) to (3.35). Mass flow rate (m_4) is given by

$$m_4 = \{Q_g - m_7 (h_7 - h_3)\} / (h_4 - h_3) \quad (3.58)$$

The concentration of LiBr in weak water concentration solution (x_4), given in subroutine 2 is calculated by

$$x_4 = (f / (f - 1)) x_3 \quad (3.59)$$

Similarly, concentration of LiBr in strong water concentration solution (x_3), given in subroutine 3 is calculated by

$$x_3 = ((f - 1) / f) x_4 \quad (3.60)$$

Rich refrigerant concentration solution circulation ratio (f) is given by equation (3.36). The thermophysical properties of air, water, water vapour and LiBr solution used in the system (concentration, temperature, pressure, specific volume, specific enthalpy and specific entropy) are given in Appendix A.

Chapter 4

Results and Discussions

4.1 Validation of computer program

The results of program for each subroutine validated with the existing data available in the literature. The results shown in Table 4.1 have been calculated for a cooling load of 1-Ton refrigeration with corresponding heat loads on absorber, condenser and generator as 4.35 kW, 3.77 kW and 4.6 kW respectively. The solution temperature at the inlet of generator being 74 °C.

Table 4.1 Validation of subroutine 1 with Arora [10]

	$P_c=P_g$ (kPa)	$P_e=P_a$ (kPa)	x_3 (wt %)	x_4 (wt %)	f (kg/kg vapour)	$m_1=m_2=m_3$ (kg/s)	$m_4=m_5=m_6$ (kg/s)	$m_7=m_8=m_9=m_{10}$ (kg/s)
Present Formulation	7.7	1.3	54.83	64.96	6.42	0.009	0.008	0.0015
Arora [13]	7.7	1.3	55.0	65.0	6.50	0.009	0.008	0.0015

The results shown in Table 4.2 have been calculated at the cooling load of 383.76 kW with corresponding heat loads on absorber, condenser and generator as 458.8 kW, 409.07 kW and 484.66 kW respectively. The solution temperature at the inlet of generator and absorber being 50 °C and 58 °C respectively.

Table 4.2 Validation of subroutine 1 with Ameen [25]

	x_3 (wt %)	x_4 (wt %)	$m_1=m_2=m_3$ (kg/s)	$m_4=m_5=m_6$ (kg/s)	$m_7=m_8=m_9=m_{10}$ (kg/s)
Present Formulation	48.0	68.0	0.56	0.39	0.162
Ameen [28]	48.0	68.0	0.55	0.39	0.162

The results shown in Table 4.3 are calculated for a rich water concentration solution circulation ratio (f) of 9.5 kg/kg vapour, condenser and absorber temperature of 29.5 °C. Figure 4.1 shows the variation of generator temperature with evaporator temperature for the tabulated data given in Table 4.3. The generator temperature decreases with increase in evaporator temperature. The generator temperature achieves a maximum value of 64.4 °C at the evaporator temperature of 8 °C. As the evaporator temperature reaches its maximum value of 12 °C, the corresponding generator temperature falls to 58.1 °C.

Table 4.3 Validation of subroutine 2 with Asdrubali and Grignaffini[19]

T_{ce} (°C)	$T_{g,}$ [Present work] (°C)	$T_{g,}$ Asdrubali and Grignaffini [19] (°C)
8	64.4	64.4
9	63.0	63.0
10	61.6	61.6
11	59.7	59.7
12	58.1	58.1

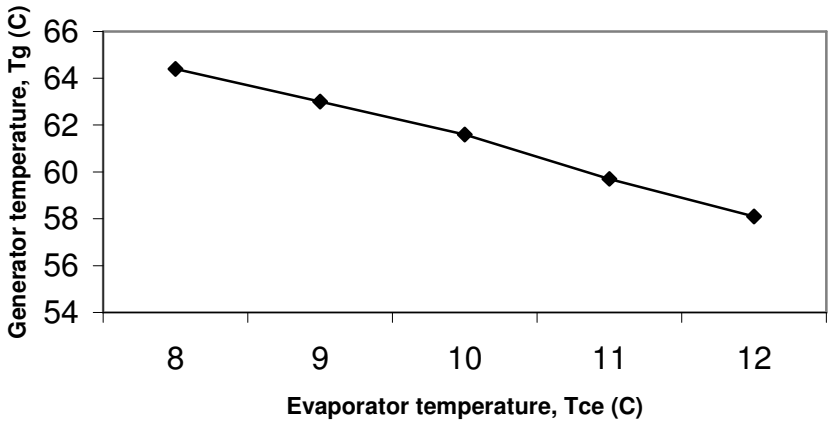

Figure 4.1 Variation of generator temperature with evaporator temperature

The results shown in Table 4.4 are calculated for a rich water concentration specific solution circulation rate (f) of 9.5 kg/kg vapour and generator temperature of 60 °C. Figure 4.2 shows the variation of evaporator temperature with condenser temperature for the tabular data given in Table 4.4. The results are drawn from subroutine 3 with a step size of 1 °C for condenser and absorber temperature. As the condenser temperature is increased, the evaporator temperature increases. The evaporator temperature reaches a maximum value of 12.8 °C from a minimum of 4.7 °C. The corresponding condenser temperatures are 31 °C and 26 °C respectively.

Table 4.4 Validation of subroutine 3 with Asdrubali and Grignaffini[19]

T_{hc}= T_a (°C)	$T_{ce,}$ [Present work] (°C)	$T_{ce,}$ Asdrubali and Grignaffini [19] (°C)
26	4.7	4.7
28	6.8	6.8
30	8.4	8.4
29	10.0	10.0
30	11.6	11.6
31	12.8	12.8

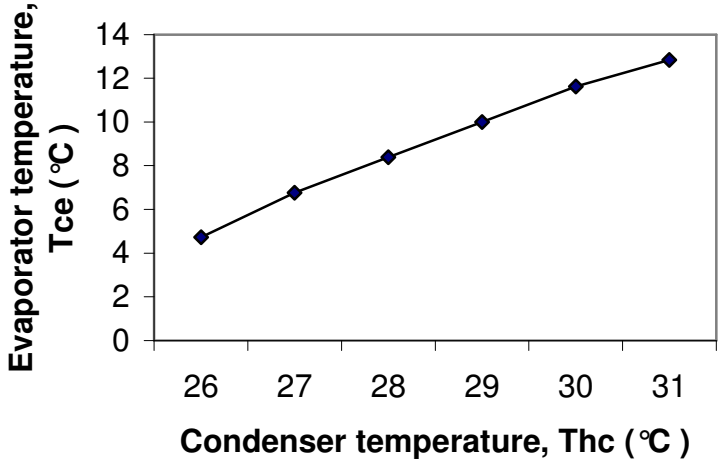

Figure 4.2 Variation of evaporator temperature with condenser temperature

For validation of exergetic calculation, computed results are compared with Misra *et al.* [24] in Table 4.5. The prediction of the present program matches satisfactorily with the available data in literature.

The results shown in Table 4.6 have been calculated for different combinations of condenser and absorber temperatures varying in the range of 20-40 °C in the step of 5 °C. The cooling load on evaporator is 4.99 kW with corresponding heat loads on absorber, condenser and generator being 19.11, 0.02 and 14.14 kW respectively. The coefficient of performance of the system is 0.3529. The specific rich water concentration solution circulation rate is 9.5 kg/kg vapour. The evaporator temperature is 10.5 °C. The mass flow rate and inlet and exit temperature of hot water in the generator being 0.99 kg/s, 73.6 °C and 70.2 °C respectively. The mass flow rates and inlet and exit temperatures of cooling water in absorber and evaporator are 0.65 kg/s and 0.36 kg/s, and 19.2 °C, 26.2 °C and 14.2 °C, 10.9 °C respectively. The mass flow rate of water vapour in the circuit is 0.002 kg/s. The pressure in the evaporator and absorber is 1.3422 kPa.

From the computed data shown in Table 4.6, it can be concluded that the LiBr concentration in the solution increases with increase in the absorber and condenser temperature. The generator temperature increases with absorber temperature for a constant value of condenser temperature. Furthermore, its value is higher for higher condenser temperature. The mass flow rate of weak water concentration LiBr solution decreases with increase in absorber and condenser temperature. The condenser and generator pressure increases with increase in condenser temperature from 2.4701 to 7.7682 kPa. The mass flow rate of weak water concentration solution becomes zero at condenser temperature 20 °C and absorber temperature of 20.83 °C below which it becomes negative because of high value of enthalpy at a higher generator temperature for a constant generator load [refer equation (3.58)]. The corresponding generator pressure is 2.4701 kPa.

Table 4.5 Validation of exergy data with Misra *et al.* [24]

States	Temperature (°C)	Pressure (kPa)	Mass flow rate (kg/s)	Chemical composition	LiBr concentration (%)	Physical exergy (kW)	Chemical exergy (kW)	Total exergy (kW)
1	34.000	0.872	0.591	Water / LiBr	56.430	19.398(19.399)	0.643(0.643)	20.041(20.043)
2	34.002	5.952	0.591	Water / LiBr	56.430	19.400(19.401)	0.643(0.643)	20.043(20.044)
3	58.350	5.952	0.591	Water / LiBr	56.430	22.073(22.075)	0.643(0.643)	22.716(22.718)
4	80.000	5.952	0.549	Water / LiBr	60.787	38.100(38.100)	0.538(0.538)	38.638(38.638)
5	53.600	0.872	0.549	Water / LiBr	60.787	34.598(34.598)	0.538(0.538)	35.136(35.136)
7	80.000	5.952	0.042	Water vapour	-	4.187(4.188)	0.105(0.106)	4.292(4.294)
8	36.000	5.952	0.042	water	-	0.040(0.039)	0.105(0.106)	0.145(0.145)
10	5.000	0.872	0.042	Water vapour	-	-7.457(-7.457)	0.105(0.106)	-7.352(-7.352)
11-12	20-12	101.325	2.981	Water	-	3.125(3.125)	0.000(0.000)	3.125(3.125)
13-14	32-27	101.325	6.352	Water	-	1.959(1.959)	0.000(0.000)	1.959(1.959)
15-16	32-27	101.325	5.041	Water	-	1.555(1.555)	0.000(0.000)	1.555(1.555)
17-18	100	101.325	0.062	Water	-	28.067(28.068)	0.000(0.000)	28.067(28.068)

Subsystems	Fuel ex. E_F (kW)	Prod. ex. E_P (kW)	Ex. Dest. E_D (kW)	Ex. Loss E_L (kW)	Ex. D. ratio Y_D (%)	Ex. L. ratio Y_L (%)	Ex. Eff. η_{ex} (%)
Generator	28.067(28.068)	20.214(20.214)	7.853(7.854)	0.000(0.000)	27.975(27.980)	0.000(0.000)	72.020(72.017)
Evaporator Assembly	19.387(19.388)	3.125(3.125)	12.748(12.750)	3.514(3.513)	45.407(45.420)	12.520(12.516)	16.119(16.120)
Solution H-X	3.502(3.501)	2.675(2.674)	0.827(0.827)	0.000(0.000)	2.945(2.946)	0.000(0.000)	76.384(76.376)
Overall sys	28.067(28.071)	3.125(3.125)	21.428(21.432)	3.514(3.513)	76.346(76.349)	12.520(12.516)	11.134(11.134)

-The bracketed terms show the values computed by Misra *et al.* [24]

Table 4.6 Output of subroutine 2

T_{hc} (°C)	T_a (°C)	x_3 (wt %)	x_4 (wt %)	T_g (°C)	m_4 (kg/s)	P_g (kPa)	P_c (kPa)
20	20	40.1090	44.8277	35.1541	-24.4372	2.4701	2.4701
20	25	44.9640	50.2539	43.2199	1.6033	2.4701	2.4701
20	30	48.5962	54.3134	50.4055	0.6914	2.4701	2.4701
20	35	51.7093	57.7927	57.2123	0.4265	2.4701	2.4701
20	40	54.5267	60.9416	63.7994	0.3050	2.4701	2.4701
25	20	40.1090	44.8277	40.5869	23.8261	3.3445	3.3445
25	25	44.9640	50.2539	48.8157	1.4485	3.3445	3.3445
25	30	48.5962	54.3134	56.0886	0.6680	3.3445	3.3445
25	35	51.7093	57.7927	62.9802	0.4203	3.3445	3.3445
25	40	54.5267	60.9416	69.6740	0.3033	3.3445	3.3445
30	20	40.1090	44.8277	46.0196	7.9783	4.4767	4.4767
30	25	44.9640	50.2539	54.4115	1.3199	4.4767	4.4767
30	30	48.5962	54.3134	61.7717	0.6458	4.4767	4.4767
30	35	51.7093	57.7927	68.7480	0.4142	4.4767	4.4767
30	40	54.5267	60.9416	75.5486	0.3015	4.4767	4.4767

35	20	40.1090	44.8277	51.4524	4.7821	5.9275	5.9275
35	25	44.9640	50.2539	60.0073	1.2116	5.9275	5.9275
35	30	48.5962	54.3134	67.4548	0.6248	5.9275	5.9275
35	35	51.7093	57.7927	74.5159	0.4080	5.9275	5.9275
35	40	54.5267	60.9416	81.4231	0.2997	5.9275	5.9275
40	20	40.1090	44.8277	56.8851	3.4104	7.7682	7.7682
40	25	44.9640	50.2539	65.6031	1.1191	7.7682	7.7682
40	30	48.5962	54.3134	73.1379	0.6049	7.7682	7.7682
40	35	51.7093	57.7927	80.2838	0.4019	7.7682	7.7682
40	40	54.5267	60.9416	87.2977	0.2977	7.7682	7.7682

The results shown in Table 4.7 have been calculated for different combinations of condenser and absorber temperatures varying in the range of 20-40 °C in the step of 5 °C for the same input data as in subroutine 2 (Table 4.6).

The LiBr concentration in the solution decreases with increase in the absorber and condenser temperature. The evaporator temperature increases with absorber temperature for a constant value of condenser temperature. Furthermore, its value is higher for higher condenser temperature. The evaporator temperature becomes zero at condenser temperature of 20 °C absorber temperature of 25.23 °C. Below this value of absorber temperature, concentration of solution is predominant and therefore evaporator

temperature is negative because of low value of absorber temperature [refer Appendix A]. The mass flow rate of weak water concentration solution increases with increase in absorber and condenser temperature. The mass flow rate of water vapour is nearly constant (0.002 kg/s). The evaporator and absorber pressure increases with condenser and absorber temperature from 0.4581 kPa to 3.9508 kPa. The condenser and generator pressure increases with increase in condenser temperature from 2.4701 to 7.7682 kPa. The mass flow rate of weak water concentration solution becomes zero at condenser temperature 40 °C and absorber temperature of 39.73 °C above which it becomes negative because of relatively high value of specific enthalpy of strong water concentration solution at a higher evaporator temperature for a constant generator load [refer equation (3.58)]. The corresponding absorber pressure is 3.4301 kPa.

Table 4.7 Output of subroutine 3

T_{hc} (°C)	T_a (°C)	T_{ce} (°C)	x_3 (wt %)	x_4 (wt %)	m_4 (kg/s)	m_{10} (kg/s)	$P_a = P_e$ (kPa)	$P_g = P_c$ (kPa)
20	20	-4.6232	52.9209	59.1469	0.3217	0.0020	0.4581	2.4701
20	25	-0.2011	52.9209	59.1469	0.3334	0.0020	0.6364	2.4701
20	30	4.2209	52.9209	59.1469	0.3460	0.0020	0.8733	2.4701
20	35	8.6429	52.9209	59.1469	0.3597	0.0020	1.1847	2.4701
20	40	13.0649	52.9209	59.1469	0.3745	0.0020	1.5898	2.4701
25	20	-0.9438	50.3941	56.3229	0.4384	0.0020	0.6027	3.3445
25	25	3.5213	50.3941	56.3229	0.4615	0.0020	0.8313	3.3445
25	30	7.9864	50.3941	56.3229	0.4873	0.0020	1.1331	3.3445
25	35	12.4514	50.3941	56.3229	0.5163	0.0020	1.5272	3.3445

25	40	16.9165	50.3941	56.3229	0.5492	0.0020	2.0367	3.3445
30	20	2.5793	47.7599	53.3787	0.6437	0.0020	0.7776	4.4767
30	25	7.0983	47.7599	53.3787	0.6973	0.0020	1.0664	4.4767
30	30	11.6173	47.7599	53.3787	0.7610	0.0020	1.4456	4.4767
30	35	16.1363	47.7599	53.3787	0.8378	0.0020	1.9382	4.4767
30	40	20.6553	47.7599	53.3787	0.9324	0.0020	2.5719	4.4767
35	20	5.9070	44.9602	50.2497	1.0537	0.0020	0.9823	5.9275
35	25	10.5043	44.9602	50.2497	1.2127	0.0020	1.3426	5.9275
35	30	15.1016	44.9602	50.2497	1.4295	0.0020	1.8141	5.9275
35	35	19.6989	44.9602	50.2497	1.7425	0.0020	2.4245	5.9275
35	40	24.2961	44.9602	50.2497	2.2339	0.0020	3.2071	5.9275
40	20	8.9487	41.9452	46.8799	1.9807	0.0020	1.2095	7.7682
40	25	13.6699	41.9452	46.8799	2.6622	0.0020	1.6537	7.7682
40	30	18.3911	41.9452	46.8799	4.0695	0.0020	2.2349	7.7682
40	35	23.1123	41.9452	46.8799	8.6823	0.0020	2.9871	7.7682
40	40	27.8335	41.9452	46.8799	-62.3054	0.0021	3.9508	7.7682

4.2 Selection of operating conditions of VAR system

The selected base operating conditions of vapour absorption refrigeration system are given below

Absorber temperature (T_a) = 34 °C

Generator temperature (T_g) = 75 °C

Evaporator temperature (T_{ce}) = 4°C

Condenser temperature (T_{hc}) = 30 °C

Heat exchanger effectiveness (ε) = 0.61

Inlet hot water temperature in generator (T_{17}) = 85 °C

Exit hot water temperature from generator (T_{18}) = 80 °C

Inlet cooling water temperature in absorber (T_{15}) = 27 °C

Exit cooling water temperature from absorber (T_{16}) = 32 °C

Inlet cooling water temperature in condenser (T_{11}) = 25 °C

Exit cooling water temperature from condenser (T_{12}) = 30 °C

Inlet temperature of chilled water in evaporator (T_{13}) = 10 °C

Exit temperature of chilled water from evaporator (T_{14}) = 2 °C

Ambient temperature of air ($T_{air, in}$) = 28 °C

Specific humidity of air (ω) = 0.0253 kg/kg dry air

Volumetric air flow rate (V) = 86 cu.m/s

Table 4.8 shows the thermodynamic properties of Water/LiBr system at the base operating conditions. The computed values of these properties at different states in the system (refer Figure 3.1) are given. The properties include temperature, pressure, LiBr concentration, chemical composition, physical exergy, chemical exergy and total exergy.

At the base operating conditions, the cooling load on the evaporator is 1973.7 kW or 561.87 Ton of refrigeration. The corresponding heat loads on condenser, generator and absorber are 1992.3 kw, 2413.7 kW and 2308.8 kW respectively. The rich water concentration solution circulation ratio is 11.2236 and coefficient of performance of the system is 0.8177.

The results of the second law analysis of the system for the base operating conditions are shown in Table 4.9. The highest exergy destruction occurs in evaporator assembly (130.4076 kW) followed by the generator (75.8892 kW) and solution heat exchanger (19.0664). Generator has the highest exergetic efficiency (80.77 %) while the exergetic efficiency of the overall system is 32.78 %.

Table 4.10 shows the results of exergy analysis for individual components of evaporator assembly at the base operating conditions. The highest contributor of exergy destruction in evaporator assembly is combined absorber and throttle valve (17.7374 kW) followed by condenser (25.6880 kW) and combined evaporator and expansion valve (86.9822 kW). The exergetic efficiency of combined evaporator and expansion valve is maximum (87.94%).

Table 4.8 Thermodynamic properties for base operating conditions of water-LiBr vapour absorption refrigeration system

States	Temperature (°C)	Pressure (kPa)	Mass flow rate (kg/s)	Chemical composition	LiBr concentration (%)	Physical exergy (kW)	Chemical exergy (kW)	Total exergy (kW)
1	34.00	0.8598	8.8925	Water / LiBr	55.2871	213.7461	9.9402	223.6863
2	34.00	4.4767	8.8925	Water / LiBr	55.2871	213.7601	9.9402	223.7003
3	59.01	4.4767	8.8925	Water / LiBr	55.2871	245.1315	9.9402	255.0717
4	75.00	4.4767	8.1002	Water / LiBr	60.6949	526.3161	7.9595	534.2755
5	45.66	4.4767	8.1002	Water / LiBr	60.6949	475.8782	7.9595	483.8377
7	75.00	4.4767	0.7923	Water vapour	-	37.4777	1.9808	39.4584
8	30.00	4.4767	0.7923	water	-	0.1604	1.9808	2.1411
10	4.00	0.8598	0.7923	Water vapour	-	-146.9101	1.9808	-144.9294[a]
11-12	25.00-30.00	101.325	95.3119	Water	-	11.6293	0.0000	11.6293
13-14	10.00-27.00	101.325	58.7242	Water	-	29.3331	0.0000	129.3331
15-16	27.00-32.00	101.325	110.4726	Water	-	28.2399	0.0000	28.2399
17-18	85.00-80.00	101.325	114.9382	Water	-	394.5514	0.0000	394.5514

a: The value is negative because both the pressure and temperature are below reference point. [24]

Table 4.9 Results of exergetic analysis for base operating conditions of the Water/LiBr vapour absorption refrigeration system

Components	Fuel ex. E_F (kW)	Prod. ex. E_P (kW)	Ex. Dest. E_D (kW)	Ex. Loss E_L (kW)	Ex.D.ratio Y_D (%)	Ex. L. ratio Y_L (%)	Ex. Eff. η_{ex} (%)
Generator (Gen.)	394.5514	318.6623	75.8892	0.0000	19.2343	0.0000	80.77
Solution pump	0.0140	0.0140	0.0000	0.0000	0.0000	0.0000	100.00
Solution heat exchanger (H-X)	50.4379	31.3714	19.0664	0.0000	4.8324	0.0000	62.19
Evaporator Assembly (Evap. ass.)	299.6098	129.3331	130.4076	39.8692	33.0521	10.1049	43.17
Overall system (Overall sys.)	394.5514	129.3331	225.3492	39.8692	57.1153	10.1049	32.78

Table 4.10 Results of exergetic analysis for the individual components of evaporator assembly

Components	Fuel ex. E_F (kW)	Prod. ex. E_P (kW)	Ex. Dest. E_D (kW)	Ex. Loss E_L (kW)	Ex. D. ratio Y_D (%)	Ex. L. ratio Y_L (%)	Ex. Eff. η_{ex} (%)
Combined evaporator (Evap.) and throttle valve (T.V.)	147.0705	129.3331	17.7374	0.0000	4.4956	0.0000	87.94
Combined absorber (Abs.)and expansion valve (E.V.)	338.9083	223.6863	86.9822	28.2399	22.0458	7.1575	66.00
Condenser (Cond.)	39.4584	2.1411	25.6880	11.6293	6.5107	2.9475	5.43

The efficiency defects or exergy destruction ratio of various components and overall system is shown in Table 4.11 to 4.18. As losses contribute to a significant amount to exergy destruction ratio, losses are also shown in the same table together with the exergetic efficiency.

Table 4.11 represents the variation of exergy destruction ratio in different components and the overall system for the condenser temperature varying between 299.15 K and 309.15 K. The exergy destruction ratio of each component (except generator) and overall system increases with condenser temperature. The losses also decrease but at a slower rate. The net effect is the reduction in plant's exergetic efficiency from 33.53 % to 28.51 %.

Table 4.11 Exergy destruction ratio expressed as percentages for various values of condenser temperature (T_{hc})

Components	Condenser temperature (K)					
	299.15	301.15	303.15	305.15	307.15	309.15
Gen.	22.4443	20.7963	19.2343	17.7839	16.4943	15.4910
H-X	3.0712	3.8591	4.8324	6.1278	8.0314	11.2709
Evap. ass.	30.7735	31.9617	33.0521	34.0016	34.7227	34.9961
Overall sys.	56.2890	56.6144	57.1153	57.9084	59.2414	61.7472
Losses	10.1843	10.1510	10.1049	10.0375	9.9308	9.7387
Ex. Eff.	33.53	33.23	32.78	32.05	30.83	28.51

The details of variation of exergy destruction ratio in evaporator assembly with condenser temperature are given in Table 4.12. The major fraction of exergy destruction ratio is in combined absorber and throttle valve, which reduces with condenser temperature, whereas the exergy destruction ratio of condenser increases with increase in its own temperature. The pie-chart of exergy destruction ratio for condenser temperatures of 299.15 K and 309.15 K are shown in Figures 4.3 and 4.4 respectively.

Table 4.12 Exergy destruction ratio in evaporator assembly expressed as percentages for various values of condenser temperature (T_{hc})

Components	Condenser temperature (K)					
	299.15	301.15	303.15	305.15	307.15	309.15
Evap.,E.V.	14.86	14.20	13.60	13.01	12.36	11.47
Abs., T.V.	84.83	75.22	66.70	59.29	53.27	49.52
Cond.	0.32	10.57	19.69	27.69	34.37	39.09

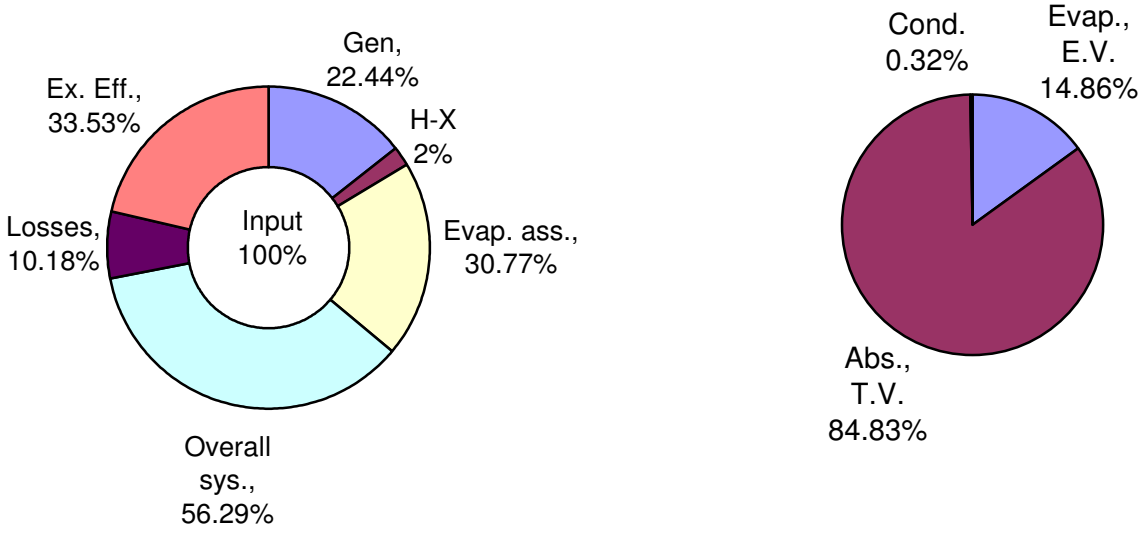

(a) System components **(b) Evaporator assembly**

Figure 4.3 Pie chart of exergy destruction ratio for a condenser temperature of 299.15 K

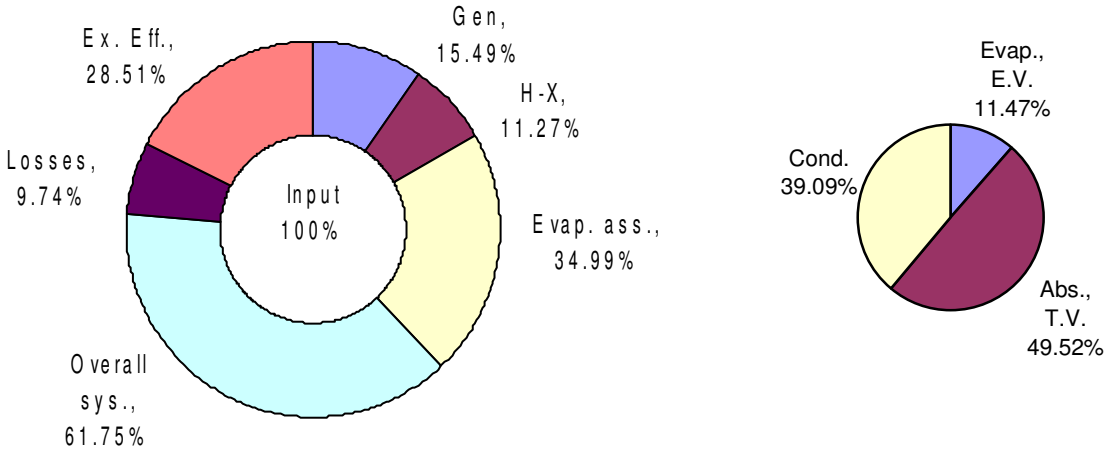

(a) System components **(b) Evaporator assembly**

Figure 4.4 Pie chart of exergy destruction ratio for a condenser temperature of 309.15 K

The pie-charts show an input of 100 % and the fractions of the input that are lost through irreversibilities in the various sub-regions of the plant. The details of the evaporator assembly are shown separately in each figure.

There is a direct casual relationship between the plant's component irreversibilities and their effects on the plant's exergetic efficiency. The fractions representing the proportion of the input lost through irreversibilities in the sub-regions are denoted (usually as percentages) by the appropriate exergy destruction ratio.

It can be seen that for T_{hc} = 279.15 K, the plant's exergetic efficiency is 33.53 % and the condenser's exergy destruction ratio is 0.32 %. If the condenser's temperature is increased to 309.15 K, the plant's exergetic efficiency is reduced to 28.51% and the condenser's exergy destruction ratio increased to 39.09 %.

Table 4.13 represents the variation of exergy destruction ratio in different components and the overall system for the evaporator temperature varying between 275.15 K and 279.15 K. The exergy destruction ratio of each component (except generator) and overall system decreases with increase in evaporator temperature. The losses increase but at a slower rate. The net effect is the increase in plant's exergetic efficiency from 31.62 % to 33.62 %.

The details of variation of exergy destruction ratio in evaporator assembly with condenser temperature are given in Table 4.14. The major fraction of exergy destruction ratio is in combined absorber and throttle valve, which increases with evaporator temperature, whereas the exergy destruction ratio of combined evaporator and expansion valve decreases with increase in its own temperature. The pie-chart of exergy destruction ratio for evaporator temperatures of 275.15 K and 279.15 K are shown in Figures 4.5 and 4.6 respectively.

Table 4.13 Exergy destruction ratio expressed as percentages for various values of evaporator temperature (T_{ce})

Components	Evaporator temperature (K)				
	275.15	276.15	277.15	278.15	279.15
Gen.	17.1342	18.1615	19.2343	20.3438	21.4842
H-X	6.1130	5.3985	4.8324	4.3744	3.9971
Evap. ass.	35.1356	34.1333	33.0521	31.9099	30.7186
Overall sys.	58.3784	57.6892	57.1153	56.6249	56.1970
Losses	9.9987	10.0560	10.1049	10.1479	10.1864
Ex. Eff.	31.62	32.25	32.78	33.23	33.62

Table 4.14 Exergy destruction ratio in evaporator assembly expressed as percentages for various values of evaporator temperature (T_{ce})

Components	Evaporator temperature (K)				
	275.15	276.15	277.15	278.15	279.15
Evap.,E.V.	22.74	18.39	13.60	8.32	2.52
Abs., T.V.	59.42	62.85	66.70	70.98	75.70
Cond.	17.84	18.75	19.69	20.70	21.78

It can be observed that for T_{ce} = 275.15 K, the plant's exergetic efficiency is 31.62 % and the exergy destruction ratio in the combined evaporator and expansion valve is 22.74 %. If the evaporator's temperature is increased to 279.15 K, the plant's exergetic efficiency is increased to 33.62 % and the exergy destruction ratio in the combined evaporator and expansion valve reduced to 2.52 %.

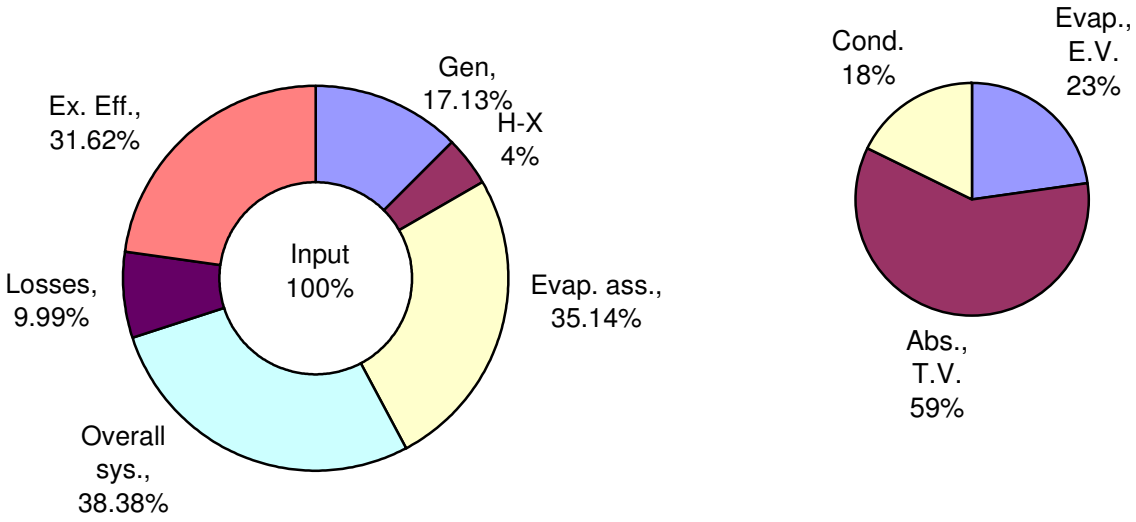

(a) System components **(b) Evaporator assembly**

Figure 4.5 Pie chart of exergy destruction ratio for an evaporator temperature of 275.15 K

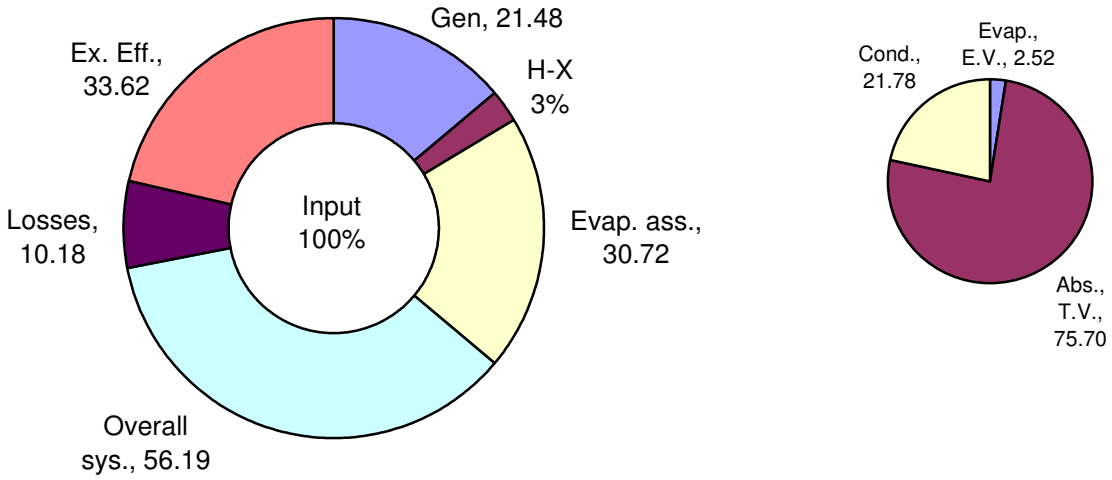

(a) System components **(b) Evaporator assembly**

Figure 4.6 Pie chart of exergy destruction ratio for an evaporator temperature of 279.15 K

Table 4.15 represents the variation of exergy destruction ratio in different components and the overall system for the absorber temperature varying between 303.15 K and 311.15 K. The exergy destruction ratio of each component (except generator) and overall system increases with increase in absorber temperature. The losses decrease continuously. The net effect is the decrease in plant's exergetic efficiency from 33.94 % to 30.83 %.

Table 4.15 Exergy destruction ratio expressed as percentages for various values of absorber temperature (T_a)

Components	Absorber temperature (K)				
	303.15	305.15	307.15	309.15	311.15
Gen.	23.3978	21.2748	19.2343	17.2876	15.4615

H-X	4.2414	4.4854	4.8324	5.3538	6.1944
Evap. ass.	28.2258	30.6747	33.0521	35.3537	37.5684
Overall sys.	55.8623	56.4318	57.1153	57.9908	59.2188
Losses	10.1977	10.1556	10.1049	10.0401	9.9491
Ex. Eff.	33.94	33.41	32.78	31.97	30.83

The details of variation of exergy destruction ratio in evaporator assembly with absorber temperature are given in Table 4.16. The major fraction of exergy destruction ratio is in combined absorber and throttle valve, which increases with absorber temperature. The pie-chart of exergy destruction ratio for absorber temperatures of 303.15 K and 311.15 K are shown in Figures 4.7 and 4.8 respectively.

Table 4.16 Exergy destruction ratio in evaporator assembly expressed as percentages for various values of absorber temperature (T_a)

Components	Absorber temperature (K)				
	303.15	305.15	307.15	309.15	311.15
Evap.,E.V.	16.49	14.94	13.60	12.40	11.25
Abs., T.V.	59.63	63.43	66.70	69.64	72.44
Cond.	23.88	21.63	19.69	17.96	16.30

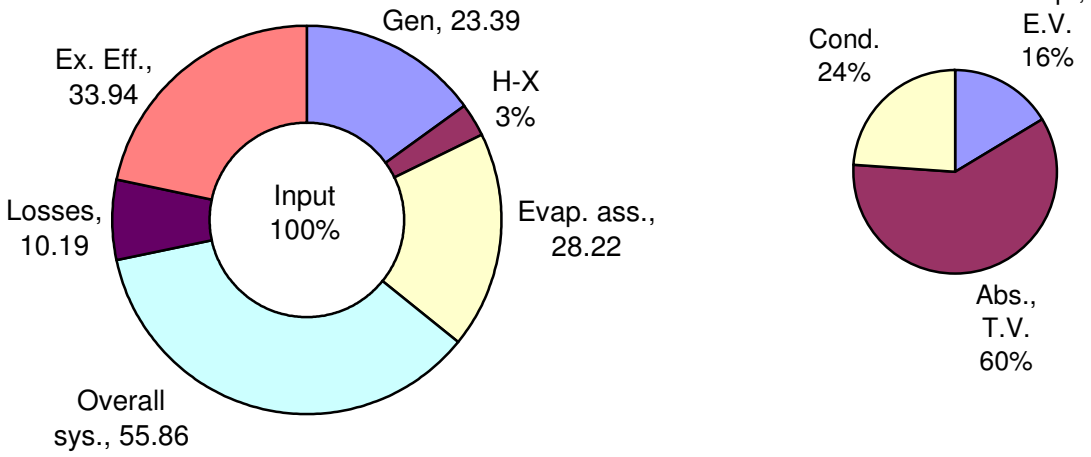

(a) System components **(b) Evaporator assembly**

Figure 4.7 Pie chart of exergy destruction ratio for an absorber temperature of 303.15 K

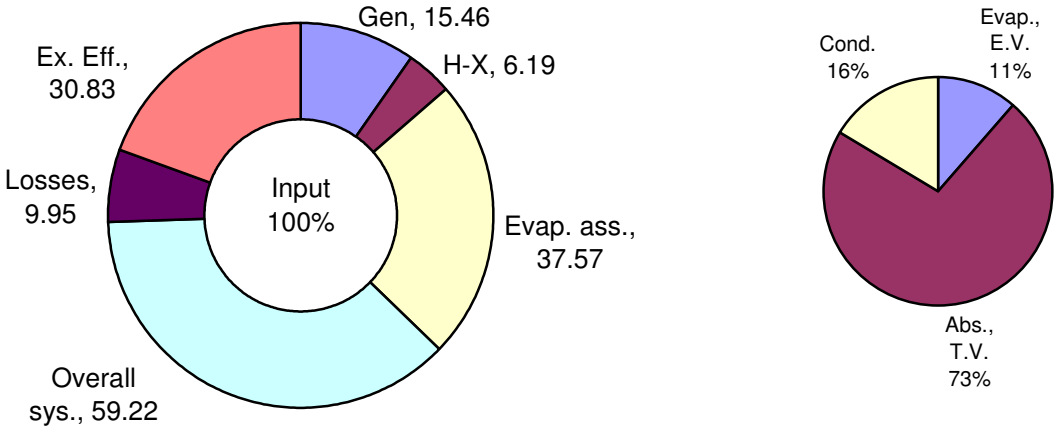

(a) System components **(b) Evaporator assembly**

Figure 4.8 Pie chart of exergy destruction ratio for an absorber temperature of 311.15 K

It is observed that for T_a = 303.15 K, the plant's exergetic efficiency is 33.94 % and the exergy destruction ratio in the combined absorber and throttle valve is 59.63 %. If the absorber's temperature is increased to 311.15 K, the plant's exergetic efficiency is reduced to 30.83 % and the exergy destruction ratio in the combined absorber and throttle valve increased to72.44 %.

Table 4.17 represents the variation of exergy destruction ratio in different components and the overall system for the generator temperature varying between 343.15 K and 363.15 K. The exergy destruction ratio of each component (except evaporator assembly) and overall system decreases with increase in generator temperature. The losses increase continuously. The net effect is the decrease in plant's exergetic efficiency from 31.21 % to 33.45 %.

Table 4.17 Exergy destruction ratio expressed as percentages for various values of generator temperature (T_g)

Components	Generator temperature (K)				
	343.15	348.15	353.15	358.15	363.15
Gen.	23.8652	19.2343	15.1296	11.4314	8.1112
H-X	6.7164	4.8324	3.8032	2.9135	1.9325
Evap. ass.	28.2236	33.0521	37.6666	42.0972	46.3889
Overall sys.	58.7994	57.1153	56.5968	56.4399	56.4307
Losses	9.9908	10.1049	10.1320	10.1321	10.1214
Ex. Eff.	31.21	32.78	33.27	33.43	33.45

The details of variation of exergy destruction ratio in evaporator assembly with generator temperature are given in Table 4.18. The major fraction of exergy destruction ratio is in combined absorber and throttle valve, which increases with generator temperature. The pie-chart of exergy destruction ratio for generator temperatures of 343.15 K and 363.15 K are shown in Figures 4.9 and 4.10 respectively.

Table 4.18 Exergy destruction ratio in evaporator assembly expressed as percentages for various values of generator temperature (T_g)

Components	Generator temperature (K)				
	343.15	348.15	353.15	358.15	363.15
Evap.,E.V.	15.17	13.60	12.11	10.89	9.89
Abs., T.V.	63.71	66.70	69.61	71.97	73.85
Cond.	21.12	19.69	18.27	17.14	16.26

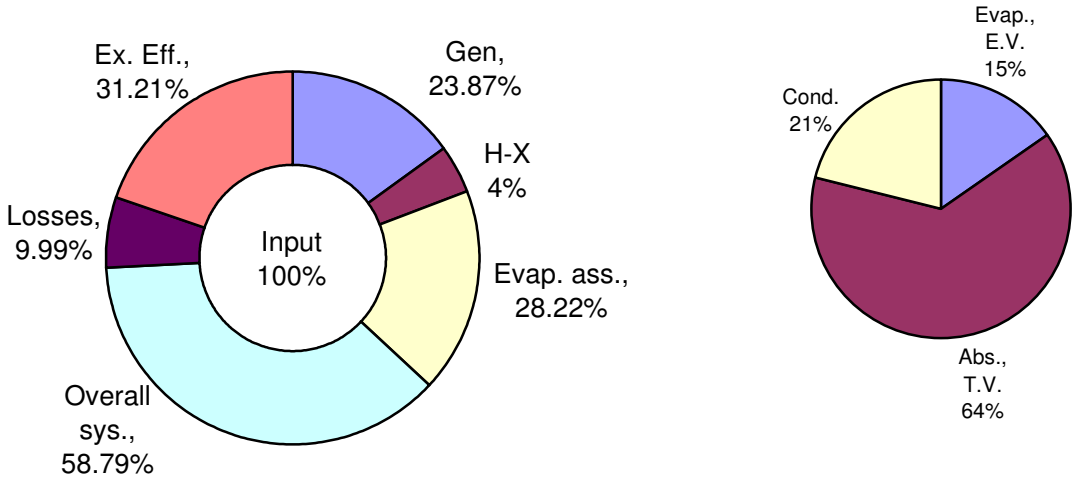

(a) System components **(b) Evaporator assembly**

Figure 4.9 Pie chart of exergy destruction ratio for a generator temperature of 343.15 K

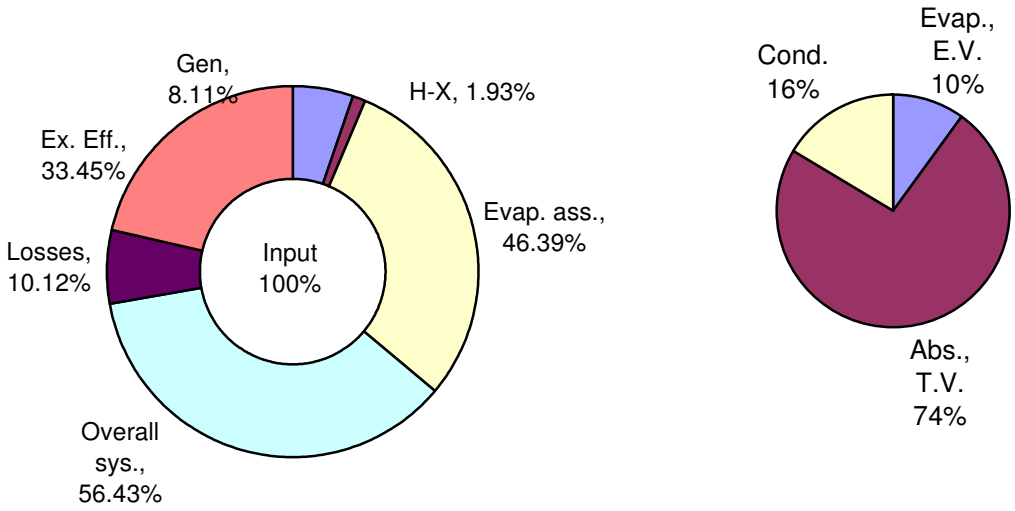

(a) System components **(b) Evaporator assembly**

Figure 4.10 Pie chart of exergy destruction ratio for a generator temperature of 363.15 K

It can be seen that for T_g = 343.15 K, the plant's exergetic efficiency is 31.21 % and exergy destruction ratio in generator is 23.86 %. As the generator temperature is increased to 363.15 K, the plant's exergetic efficiency increased to 33.45 % with a corresponding reduction in exergy destruction ratio in generator to 8.11 %.

Tables 4.19 to 4.22 show the effect of varying temperature of condenser, evaporator, absorber and generator on their individual irreversibility rates as well as total irreversibility rate of the plant. The effect of the variation of temperatures of different components of the system on plant's exergetic efficiency and rich water concentration solution circulation ratio (f) is also indicated.

Table 4.19 Irreversibilities, plant's exergetic efficiencies and rich water concentration solution circulation ratios for stated values of T_{hc}, (T_{ce} = 277.15 K, T_g = 348.15 K, T_a = 307.15 K)

Condenser temperature (K)	Total plant's irreversibility rate (kW)	Condenser's irreversibility rate (kW)	Evaporator assembly's irreversibility rate (kW)	Plant's exergetic efficiency (%)	Circulation ratio f
299.15	217.1416	0.3748	118.7125	33.5267	8.3573
301.15	220.3164	13.1501	124.3796	33.2346	9.5549
303.15	225.3492	25.6880	130.4076	32.7798	11.2236
305.15	233.6511	37.9928	137.1910	32.0541	13.7205
307.15	248.5380	50.0688	145.6738	30.8278	17.8840
309.15	280.0710	61.9204	158.7344	28.5140	26.2571

Table 4.20 Irreversibilities, plant's exergetic efficiencies and rich water concentration solution circulation ratios for stated values of T_{ce}, (T_{hc} = 303.15 K, T_g = 348.15 K, T_a = 307.15 K)

Evaporator temperature (K)	Total plant's irreversibility rate (kW)	Evaporator's irreversibility rate (kW)	Evaporator assembly's irreversibility rate (kW)	Plant's exergetic efficiency (%)	Circulation ratio f
279.15	216.2071	2.9802	118.1836	33.6166	9.1217
278.15	220.4062	10.3370	124.2059	33.2272	10.0695
277.15	225.3492	17.7374	130.4076	32.7798	11.2236
276.15	231.3185	25.1821	136.8654	32.2548	12.6616
275.15	238.7591	32.6715	143.6995	31.6229	14.5060

Table 4.21 Irreversibilities, plant's exergetic efficiencies and rich water concentration solution circulation ratios for stated values of T_a, (T_{ce} = 277.15 K, T_g = 348.15 K, T_{hc} = 303.15 K)

Absorber temperature (K)	Total plant's irreversibility rate (kW)	Absorber's irreversibility rate (kW)	Evaporator assembly's irreversibility rate (kW)	Plant's exergetic efficiency (%)	Circulation ratio f
303.15	212.8717	64.1330	107.5584	33.9399	7.9541
305.15	218.4355	75.3096	118.7351	33.4126	9.3331
307.15	225.3492	86.9760	130.4076	32.7798	11.2236
309.15	234.6051	99.6001	143.0255	31.9691	13.9882
311.15	248.4089	114.1652	157.5907	30.8320	18.4350

Table 4.22 Irreversibilities, plant's exergetic efficiencies and rich water concentration solution circulation ratios for stated values of T_g, (T_{ce} = 277.15 K, T_{hc} = 303.15 K, T_a = 307.15 K)

Generator temperature (K)	Total plant's irreversibility rate (kW)	Generator's irreversibility rate (kW)	Evaporator assembly's irreversibility rate (kW)	Plant's exergetic efficiency (%)	Circulation ratio f
363.15	218.2006	31.3635	179.3719	33.4479	5.6862
358.15	218.3667	44.2283	162.8745	33.4279	6.6756
353.15	220.0050	58.8124	146.4189	33.2712	8.2598
348.15	225.3492	75.8892	130.4076	32.7798	11.2236
343.15	243.6649	98.8912	116.9584	31.2097	18.8280

The variation of temperatures in condenser, evaporator, absorber and generator affects not only the component's irreversibility rates, but the irreversibility rate of the plant as whole.

The results shown in Tables 4.19 to 4.22 are used to plot the graphs of Figures 4.11 to 4.14, with variables T_{hc}, T_{ce}, T_a and T_g respectively. The mean slopes of the curves give the Coefficient of Structural Bonds. The slope of the line in Figure 4.11 is increasing continuously indicating increased rates of irreversibility at lower evaporator temperatures. The slope achieves a minimum of 0.25 and a maximum of 1.23. The average CSB of the condenser is found to be 1.04. The slope of the line shown in Figure 4.12 is increasing continuously and its value lies between a minimum of 0.57 and a maximum of 0.99. The average CSB of evaporator is found to be 0.76. Similar trends are found in absorber and generator depicting larger rates irreversibility at higher absorber temperature and lower generator temperature. Average CSB of absorber and generator are 0.69 and 0.31 respectively.

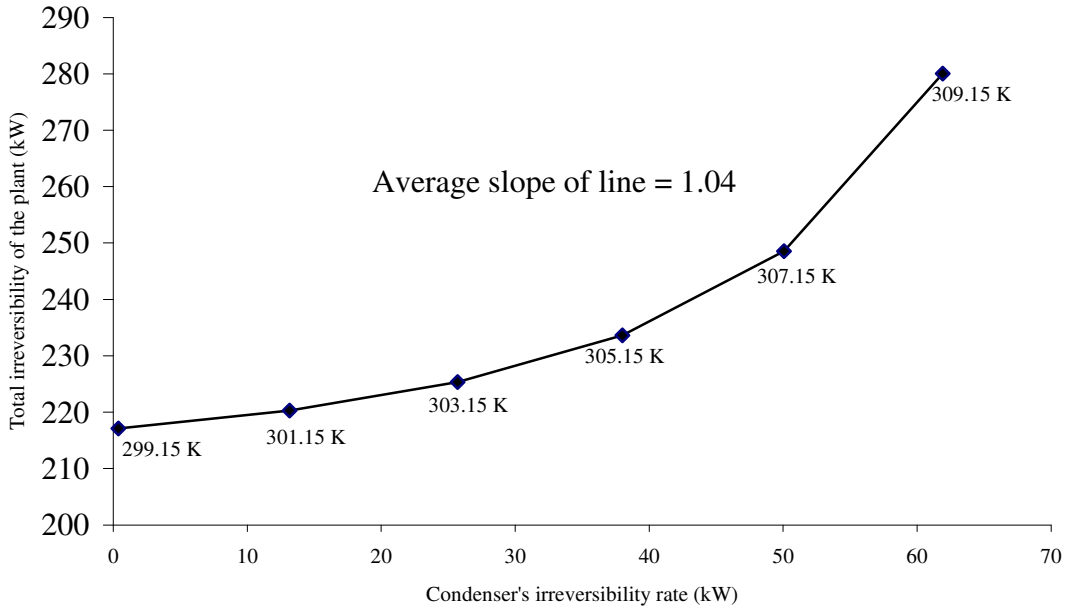

Figure 4.11 Plot for determining the CSB of the condenser with $E_{D,\,c}$ as variable and (T_{ce} = 277.15 K, T_a = 307.15 K, T_g = 348.15 K).

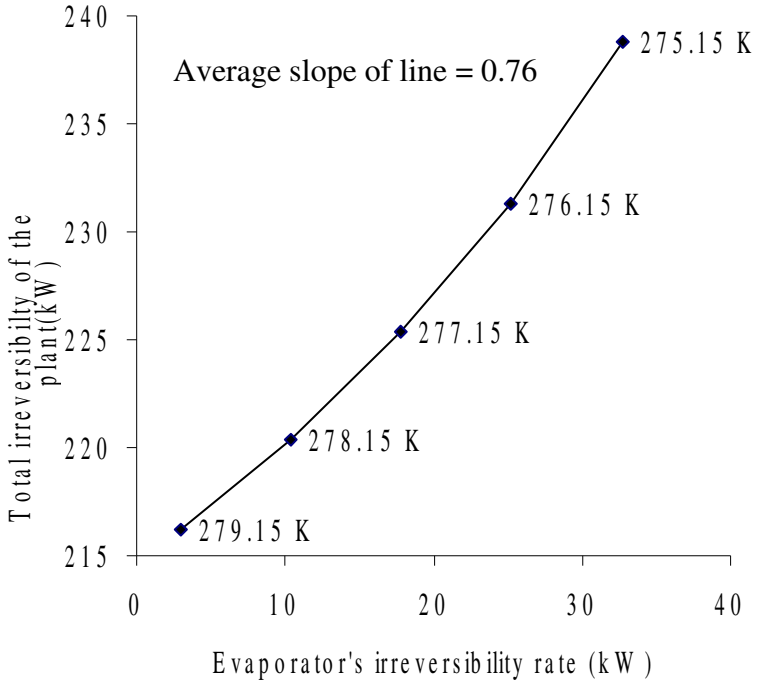

Figure 4.12 Plot for determining the CSB of the evaporator with $E_{D,e}$ as variable and (T_{hc} = 303.15 K, T_a = 307.15 K, T_g = 348.15 K).

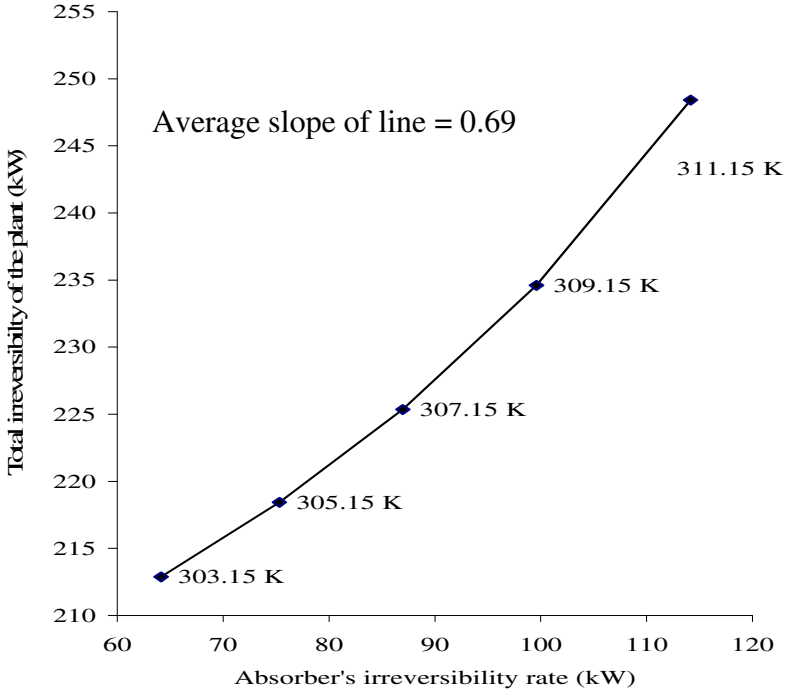

Figure 4.13 Plot for determining the CSB of the absorber with $E_{D,\,a}$ as variable and (T_{ce} = 277.15 K, T_{hc} = 303.15 K, T_g = 348.15 K).

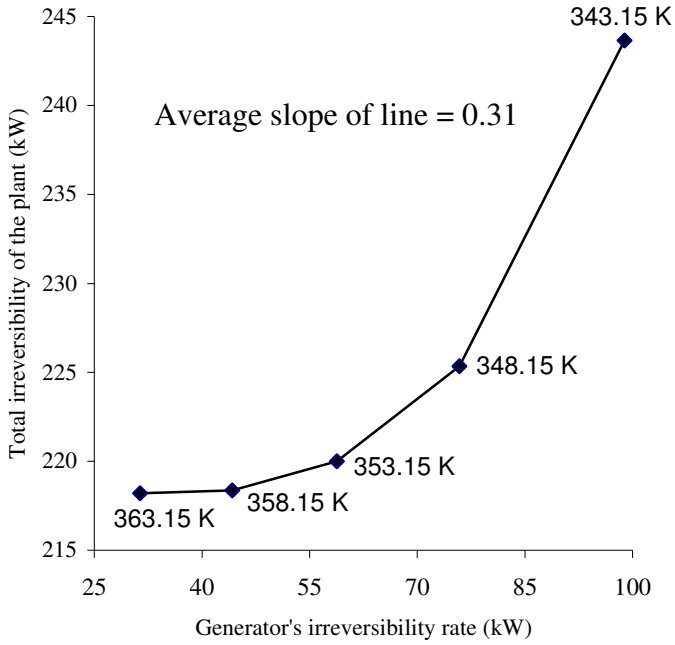

Figure 4.14 Plot for determining the CSB of the generator with $E_{D,\,g}$ as variable and (T_{ce} = 277.15 K, T_a = 307.15 K, T_{hc} = 303.15 K).

From Tables 4.19 to 4.22, it can be seen that the irreversibility rate in evaporator assembly and rich water concentration LiBr solution circulation ratio are increasing continuously with condenser temperature, with corresponding minimum and maximum values of (118.3573 kW, 158.7344 kW) and (8.3573 , 26.2571) respectively. The irreversibility rate in evaporator assembly and rich water concentration LiBr solution circulation ratio are increasing continuously with decrease in evaporator temperature , with corresponding minimum and maximum values of (118.1836 kW, 143.6995 kW) and (9.1217, 14.5060) respectively. In case of absorber, the irreversibility rate in evaporator assembly and rich water concentration LiBr solution circulation ratio are increasing continuously with absorber temperature, with corresponding minimum and maximum values of (107.5584 kW, 157.5907 kW) and (7.9541 , 18.4350) respectively. With decrease in generator temperature, the irreversibility rate in evaporator assembly is

decreasing from a maximum of 179.3719 kW to a minimum of 116.9584 kW. On the other hand, rich water concentration LiBr solution circulation ratio is increasing continuously with corresponding decrease in generator temperature and attains minimum and maximum values of 5.6862 and 18.8280 respectively.

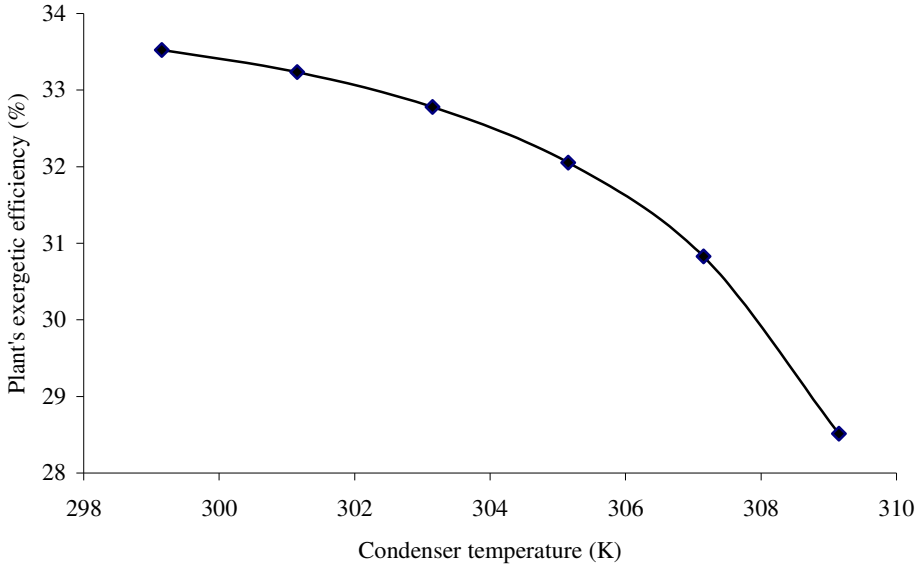

Figure 4.15 Plant's exergetic efficiency dependence upon the condenser temperature

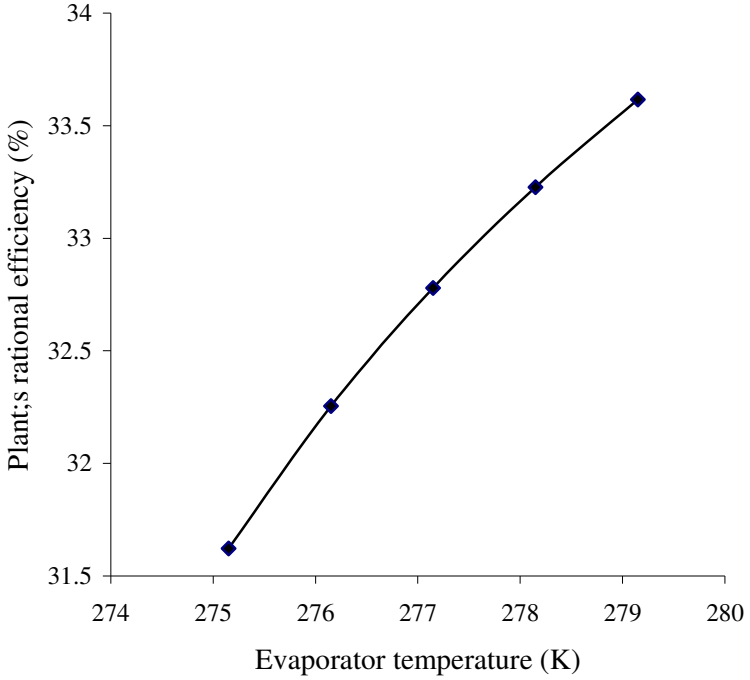

Figure 4.16 Plant's exergetic efficiency dependence upon the evaporator temperature

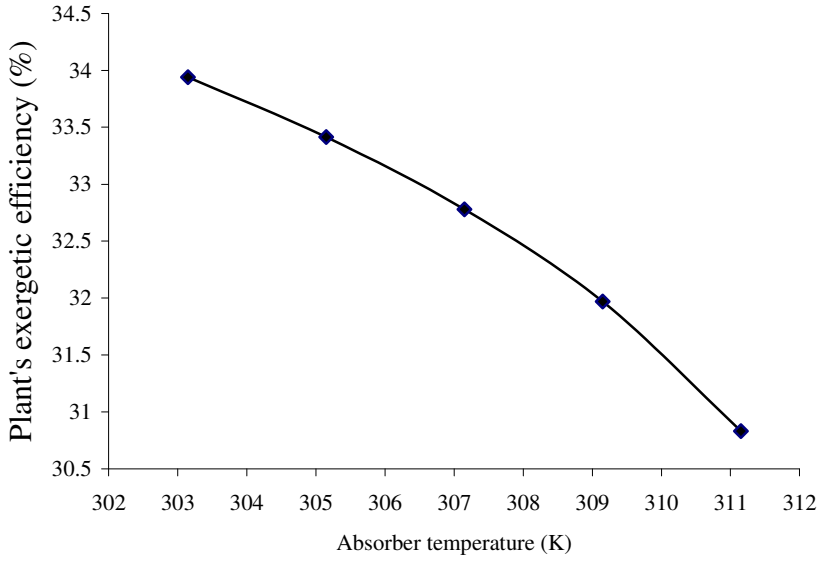

Figure 4.17 Plant's exergetic efficiency dependence upon the absorber temperature

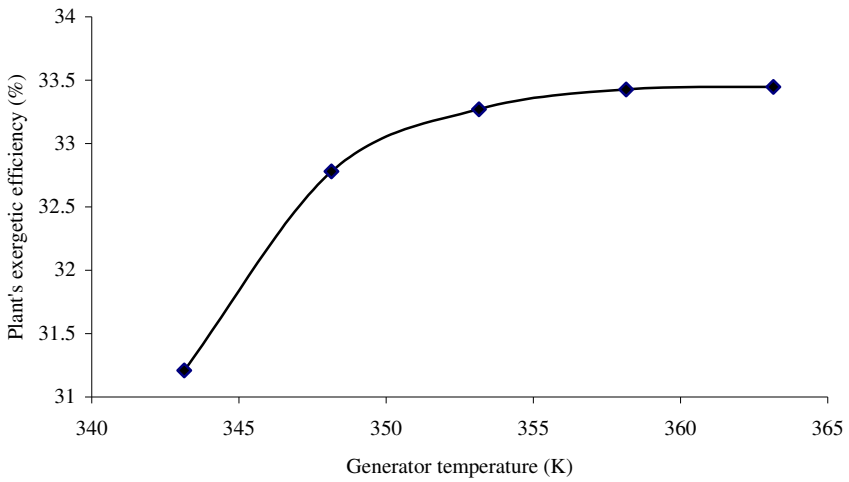

Figure 4.18 Plant's exergetic efficiency dependence upon the generator temperature

Finally, Figures 4.15 to 4.18 show the effects of varying condenser, evaporator, absorber and generator temperatures on plant's exergetic efficiency. It can be seen that plant's exergetic efficiency reduces with increase in condenser and absorber temperatures. While in case of evaporator and generator, plant's efficiency increases with increase in evaporator and generator temperatures. It is clear from results, the range of temperature variation of the components of the plant is to be optimized to achieve a satisfactory design of the plant.

Chapter 5
Conclusions and Recommendations for Future Work

From the thermodynamic analysis of single-effect Water/LiBr Vapour Absorption Refrigeration System, following conclusions can be given:

1. The coefficient of performance of the system is 0.8177. The cooling load on evaporator is 1973.7 kW or 561.87 Ton of refrigeration. The heat loads on generator, condenser and absorber are 2413.7 kW, 1992.3 kW and 2308.8 kW respectively.

2. The exergy destruction ratio and exergy loss ratio of the system are 57.1153 % and 10.1049 % respectively. The exergetic efficiency of the plant is 32.78 %.

3.The exergy destruction ratio of the plant increases with increase of condenser temperature (from 58.3784 kW to 56.1970 kW) and absorber temperature (from 55.8623 kW to 59.2188 kW) for condenser and absorber temperatures varying between 30°C to 36 °C and 30°C to 38 °C respectively. While in case of evaporator and generator reverse pattern is followed.

4. Plant's irreversibility rate is increasing with increase of condenser and absorber temperature while it decreases with increase of evaporator and generator temperatures.

5. Exergetic efficiency of the plant decreases as the condenser and absorber temperatures increase, while for evaporator and generator, it increases with increase in their corresponding temperatures.

Recommendations for future work

1. Second law analysis is an important tool in the thermoeconomic optimization of a refrigeration plant. Thermoeconomic optimization can be performed to design the components of the system.

2. Power augmentation in Gas Turbine Power Plants by the use of Water/LiBr Vapour Absorption refrigeration System can be done.

Appendix A

1. Temperature of generator at solution concentration x_4 and condenser temperature T_{hc} (refrigerant temperature) is given by [25]

$$T_g=(124.937-7.71649.* x_4+.152286.*(x_4.^2)-7.95090* (10^-4).*(x_4.^3))+T_{hc}.*(-2.00755+.16976.* x_4- 3.133326*(10^-3).*(x_4.^2)+1.97668*(10^-5).*(x_4.^3)) \quad (A.1)$$

where,

T_g= Generator temperature in °C.

x_3= concentration of LiBr-water solution in wt%.

T_{hc}= Condenser temperature in °C.

2. Temperature of evaporator at solution concentration x_3 and absorber temperature T_a (solution temperature) is given by [25]

$$T_{ce}=(T_a-(124.937-7.71649.*x_3+.152286*(x_3.^2)-7.95090*(10^-4).*(x_3.^3)))/((-2.00755+.16976.* x_3-3.133326*(10^-3)*(x_3.^2)+1.97668*(10^-5)*(x_3.^3))) \quad (A.2)$$

3. Concentration of LiBr (x_3) in strong water concentration solution at absorber temperature T_a and evaporator temperature T_{ce} is given by the root of equation (A.2)

4. Concentration of LiBr (x_4) in weak water concentration solution at generator temperature T_g and condenser temperature T_{hc} is given by the root of equation (A.1)

5. Specific enthalpy of LiBr-water solution is given by [23]

h=(-954.8+47.7739.*(x)-1.59235.*(x.^2)+0.0209422.*(x.^3)-0.00007689.*(x.^4))
+(T+273.15).*(-0.3293+0.04076.*(x)-0.0000136.*(x.^2)-0.0000071366.
(x.^3))+((T+273.15).^2)(0.0074285-0.00015144.*(x)+0.0000013555.*(x.^2))
-((T+273.15).^3)*0.000002269 (A.3)

where,

h= Specific enthalpy in kJ/kg.

x= Concentration of LiBr in the solution in wt%.

T= Temperature in °C.

6. Specific enthalpy of water is given by [26]

h= (-2.844699*10^-2+4.211925*T-1.017034*10^-3*(T^2)+1.311054*10^-
5*(T^3)-6.756469*10^-8*(T^4)+1.724481*10^-10*(T^5))

(A.4)

7. Latent heat of vapourization of water is given by [26]

h_{fg} = (2500.304-2.2521025*T-0.021465847*(T^1.5)+3.1750136*10^-4*(T^2.5)-
2.8607959*10^-5*(T^3))

(A.5)

8. Specific enthalpy of saturated water vapour is given by

h = (-2.844699*10^-2+4.211925*T-1.017034*10^-3*(T^2)+1.311054*10^-

5*(T^3)-6.756469*10^-8*(T^4)+1.724481*10^-10*(T^5))+(2500.304
-2.2521025*T-0.021465847*(T^1.5)+3.1750136*10^-4*(T^2.5)-2.8607959*
10^-5*(T^3))

(A.6)

9. Specific enthalpy of superheated water vapour is given by [10]

h = (-2.844699*10^-2+4.211925*T-1.017034*10^-*(T^2)+1.311054*10^-
5*(T^3)-6.756469*10^-8*(T^4)+1.724481*10^-10*(T^5))+(2500.304
-2.2521025*T-0.021465847*(T^1.5)+3.1750136*10^-4*(T^2.5)-2.8607959*
10^-5*(T^3))+C_{pvs}.*(T_s-T) (A.7)

where,

C_{pvs} = Specific heat of superheated water vapour

= 1.88 kJ/kgK

T_s = Temperature of superheated water vapour in °C

10. Specific entropy of Libr-water solution is given by [23]

s=(5.127558*10^-1-1.393954*10^-2*x+2.924145*10^-5*x^2+9.035697*10^-
7*x^3)+(1.22678*10^-2*T-9.15682*10^-5*x*T+1.820453*10^-8*x^2*T-
7.991806*10^-10*x^3*T)+(-1.364895*10^-5*T^2+1.068904*10^-7*x*T^2-
1.381109*10^-9*x^2*T^2+1.529784*10^-11*x^3*T^2)+(1.021501*10^-
8*T^3) (A.8)

11. Specific entropy of water is given by [41]

$$s = 4.191*\log((T+273.15)/(273.15+0.01)) \quad \text{(A.9)}$$

12. Specific entropy of saturated water vapour is given by

$$s = (h_{fg}/(T+273.15)+ 4.191*\log((T+273.15)/(273.15+0.01))) \quad \text{(A.10)}$$

12. Specific entropy of superheated water vapour is given by [10]

$$s = (h_{fg}/(T+273.15)+ 4.191*\log((T+273.15)/(273.15+0.01))) + C_{pvs} *\log((T_s+273.15) /(T+273.15)) \quad \text{(A.11)}$$

12. Pressure in the generator (or condenser) is given by [25]

$$P_c= P_g =10\text{^}(7.05-(1596.49/(Thc+273.15))-(104095.5/((Thc+273.15).\text{^}2))) \quad \text{(A.12)}$$

13. Pressure in the evaporator (or absorber) is given by[25]

$$P_e = P_a = 10\text{^}(7.05-(1596.49/(Tce+273.15))-(104095.5/((Tce+273.15).\text{^}2))) \quad \text{(A.13)}$$

14. Specific volume of water vapour is given by (A.14)

$$v=(((0.2871+(0.462.*\omega))).*(T/P_{atm}))$$

where,

ω = Specifc humidity in kg/kg of dry air.

P_{atm} = Atmospheric pressure in kPa.

15. Specifc heat of air is given by

C_{pa}= ((6.557+1.477*(10)^-3.*(T+273.15)-0.2148*(10)^-6*(T+273.15).^2)
(4.187/29)+ ω (6.97+3.464(10)^-3.*(T+273.15)-0.4833*(10)^-6*(
T+273.15).^2)*(4.187/18)) (A.15)

16. Specific heat of water is given by

C_{ps} = 4.2174356+(-.0056181625.*(T1-273))+(.0012992528.*((T1-273).^1.5))+(-
.00011535353.*((T1-273).^2))+(4.14964*10^-6).*((T1-273)).^2.5 (A.16)

References

[1]. Ravi Kumar N., Dr. Rama Krishna K., Dr. Sita Rama Raju A.V., "Improved Gas Turbine Efficiency Using Spray Coolers and Through Alternative Regenerator Configuration", ISHMT-ASME, Heat and Mass Transfer Conference, (Jan 2006), Pp.-1819-1824

[2]. Velasco Gomez E., Rey Martinez F.J., Varela Diez F., Molina Leyva M.J., Herrero Martin R., "Description and Experimental Results of a Semi-indirect Ceramic Evaporative Cooler", International Journal of Refrigeration, Vol.28, (March 2005), Pp. 654-662.

[3]. Datta S., Sahgal P.N., Subrahmaniyam S., Dhingra S.C., Kishore V.V.N., "Design and Operating Characteristics of Evaporative Cooling Systems", International Journal of Refrigeration, Vol.10, (July 1987), Pp.205-208.

[4]. Adrian Bejan, George Tsatsaronis, Michael Moran, "Thermal Design and Optimization", John Wiley and Sons, Inc., (1996), Pp.114-163.

[5]. Al-Amiri Abdalla M., Zamzam Montaser M., "Systematic Assessment of Combustion Turbine Inlet Air-Cooling Techniques", Journal of Engineering for Gas Turbine and Power, Vol.127, (Jan2005), Pp.159-169.

[6]. Dawoud B., Zurigat Y.H., Bortmany J., "Thermodynamic Assessment of Power Requirements and Impact of Different Gas-Turbine Inlet Air-Cooling Techniques at Two Different Locations in Oman", Applied Thermal engineering Vol.25, (2005), Pp.1579-1598.

[7]. Alhazmy M.M., Najjar Y.S.H., "Augmentation of Gas Turbine Performance Using Air Coolers", Applied Thermal Engineering, Vol.24, (2004), Pp.415-429.

[8]. De Lucia M., Lanfranchi C., Boggio V., "Benefits of Compressor Inlet Air Cooling for Gas Turbine Cogeneration Plants', Journal of Engineering for Gas Turbine and Power, Vol.118, (July1996), Pp.598-602.

[9]. Bhargava R., Meher-Homji C.B., "Parametric Analysis of Existing Gas Turbines with Inlet Evaporative and Overspray Fogging", Journal of Engineering for Gas Turbines and Power, Vol.127, (Jan 2005), Pp.145-158.

[10]. Arora C.P., "Refrigeration and Air Conditioning", Tata McGraw-Hill Publishing Company Limited, 1983, Pp. 53-104, 304-325, 337-406.

[11]. Moran M.J., "Availability Analysis", ASME Press, New York, NY, (1989), Pp.123-143.

[12]. Cammarata G., Fichera A., Mammino L., Marletta L., "Exergonomic Optimization of an Air-Conditioning System", Journal of Energy Resources Technology, Vol.119, (Mar1997), Pp.62-69.

[13]. Ait-Ali M.A., "Optimum Power Boosting of Gas Turbine Cycles with Compressor Inlet Air Refrigeration", Journal of Engineering for Gas Turbines and Power, Vol.119, (Jan1997), Pp.124-133.

[14]. Nikolaidis C., probert D., "Exergy-Method Analysis of a Two-Stage Vapour Compression Refrigeration-Plant's Performance", Applied Energy, Vol.60, (1998), Pp.241-256.

[15]. Haselden Geoffrey G., Chen J., "A Computer Simulation Program for Mixed-Refrigerant Air-Conditioning", International Journal of Refrigeration, Vol.17 Number 5, (1994), Pp.343-350.

[16]. Yunho Hwang, “Potential energy benefits of integrated refrigeration system with microturbine and absorption chiller”, International Journal of Refrigeration, Vol.27, (2004), Pp.816-829.

[17]. Horuz I., Callander T.M.S., “Experimental Investigation of a Vapour Absorption Refrigeration System”, International Journal of Refrigeration, Vol.27, (2004), Pp.10-16.

[18]. Waked A.M., “Second Law Analysis of a Cogeneration Power-Absorption Cooling Plant”, Heat Recovery Systems & CHP, Vol.11, (1991), Pp.113-120.

[19]. Asdrubali F., Grignaffini S., “Experimental Evaluation of the Performances of a H_2O-LiBr Absorption Refrigerator under Different Service Conditions”, International Journal of Refrigeration, Vol.28, (2005), Pp.489-497.

[20]. Gershon Grossman, Abdi Zaltash, “ABSIM-Modular Simulation of Advanced Absorption Systems”, International Journal of Refrigeration, Vol.24, (2001), Pp.531-543.

[21]. Chan Woo Park, Jin Hee Jeong, Yong Tae Kang, “Energy Consumption Characteristics of Absorption Chiller during the Partial Load Operation”, International Journal of Refrigeration, Vol.27, (2004), Pp.948-954.

[22]. Antonio De Lucas, Marina Donate, Carolina Molero, Jose Villasenor, Rodriguez Juan F., “Performance Evaluation and simulation of a New Absorbent for an Absorption Refrigeration System”, International Journal of Refrigeration, Vol.27, (2004), Pp.324-330.

[23]. Kaita Y., “Thermodynamic Properties of Lithium Bromide-Water Solutions at High Temperatures”, International Journal of refrigeration, Vol.24, (2001), Pp.374-390.

[24]. Misra R.D., Sahoo P.K., Gupta A., "Thermoeconomic Optimization of a Single Effect Water/LiBr Vapour Absorption Refrigeration System", International Journal of Refrigeration, Vol.26, (2003), Pp.158-169.

[25]. Ahmadul Ameen, "Refrigeration and air conditioning", Prentice-Hall of India Pvt. Ltd., 2006, Pp.79-93.

[26]. Popiel C.O. and Wojtkowiak J., "Simple formulas for thermophysical properties of liquid water for heat transfer calculations (from 0°C to 150°C)", heat transfer engineering, Vol.19, (1998), Pp.87-101.

[27]. Kakaras E., Doukelis A., Prelipceanu A., Karellas S., "Inlet air cooling methods for Gas Turbine based Power Plants", Journal of Engineering for Gas Turbines and Power, Vol.128, (April 2006), Pp.312-317.

[28]. Craig Cortes, P.E. and Daniel Willems, P.E., "Gas turbine inlet air cooling techniques: An overview of current technologies", Siemens Westing House, PowerGen 2003-Las Vegas, Nevada, Sept. (2003).

[29]. Talbi M.M., Agnew B., "Exergy analysis: an absorption refrigerator using lithium bromide and water as the working fluids", Applied Thermal Engineering, Vol.20, (2000), Pp.619-630.

[30]. Onder Kizilkan, Arzu Sencan, Kalogirou Soteris A., "Thermoeconomic optimization of a LiBr absorption refrigeration system", Chemical Engineering and Processing, Vol.xxx, (2006), Pp.1-9.

[31]. Florides G.A., Kalogirou S.A., Tassou S.A., Wrobel L.C., "Modelling, simulation and warming impact assessment of a domestic-size absorption solar cooling system", Applied Thermal Engineering, Vol.22, (2002), Pp.1313-1325.

[32]. Joudi Khalid A., Lafta Ali H., "Simulation of a simple absorption refrigeration system", Energy Conversion and Management, Vol.42, (2001), Pp.1575-1605.

[33]. Misra R.D., Sahoo P.K., Gupta A., "Thermoeconomic evaluation and optimization of a double-effect H_2O/LiBr vapour-absorption refrigeration system", International Journal of Refrigeration, Vol.28, (2005), Pp.331-343.

[34]. Xu S.M., Zhang L., Xu C.H., Liang J., Du R., "Numerical simulation of an advanced energy storage system using H_2O-LiBr as working fluid, Part 1: System design and modeling", International Journal of Refrigeration, Vol.30, (2007), Pp.354-363.

[35]. Xu S.M., Xu C.H., Zhang L., Liang J., Du R., "Numerical simulation of an advanced energy storage system using H_2O-LiBr as working fluid, Part 2: System simulation and analysis", Vol.30, (2007), Pp. 364-376.

[36]. Tozer Robert M., James Ron W., "Fundamental thermodynamics of ideal absorption cycles", International Journal of Refrigeration, Vol.20, (1997), Pp.120-135.

[37]. Garcia-Valladares O., Perez-Segarra C.D., Rigola J., "Numerical simulation of double-pipe condensers and evaporators", International Journal of Refrigeration, Vol.27, (2004), Pp.656-670.

[38]. Robert Tozer, Athar Syed, Graeme Maidment, "Extended temperature-entropy (T-s) diagrams for aqueous lithium bromide absorption refrigeration cycles", International Journal of Refrigeration, Vol.28, (2005), Pp.689-697.

[39]. Ondryas I.S., Wilson D.A., Kawamoto M., Haub G.L., "Options in Gas Turbine Power Augmentation Using inlet Air Chilling", Journal of Engineering for Gas Turbines and Power, Vol.113, (April 1991), Pp.203-211.

[40]. Kakaras E., Doukelis A., Karellas S., “Compressor Intake-Air Cooling in Gas Turbine Plants”, Journal of Energy, Vol.29, (2004), Pp.2347-2358.

[41]. Fernandes J.L.M., “Correlations for fast computation of thermodynamic properties of saturated water and steam”, International Journal of Energy Research”,Vol.19, (1995), Pp.507-514.